THE MATHEMATICS CLINIC

PROBABILISTIC POSITION-FIXING

FINAL REPORT OF THE 1985-86 CLAREMONT GRADUATE SCHOOL
CLAREMONT MCKENNA COLLEGE MATHEMATICS CLINIC

Sponsored by the JET PROPULSION LABORATORY

TEAM MEMBERS

Spring 1986	Fall 1985
Steve Burnett (Team Leader)	Steve Burnett (Team Leader)
Laurie Louie	Paul Cliff
Eric Mulfinger	Yvette Lohse
Matt Porta	Eric Mulfinger
Dana Price	Diana Thomas
Andy Smith	
Drea Solan	
Mark Yamada	

FACULTY ADVISOR: Professor John Ferling
FACULTY CONSULTANT: Professor Larry Knop (Fall 1985)
JPL LIAISONS: Jim Gillis, Dr. Anne Griesel

June 1986
THE CLAREMONT GRADUATE SCHOOL

This report was prepared for the Jet Propulsion Laboratory, California Institute of Technology, sponsored by the National Aeronautics and Space Administration.

TABLE OF CONTENTS

ACKNOWLEDGEMENT

The Clinic team would like to express its sincere appreciation for the help and cooperation of the sponsor, the Jet Propulsion Laboratory. In particular, the team wishes to acknowledge the JPL liaisons, Jim Gillis and Dr. Anne Griesel.

I INTRODUCTION AND OVERVIEW

This is the final report of the 1985-86 Claremont Graduate School and Claremont McKenna College Mathematics Clinic concerning a problem proposed by the Intelligence Analysis Group at the Jet Propulsion Laboratory. The problem is to determine confidence regions for the location of objects or emitters on which bearings are taken from two or more sensors whose positions are known.

This problem for the two-sensor case was studied by a different clinic during the 1984-85 academic year. This clinic studied the classical approach to determining such regions which involved the assumption that an error of observation of the line of bearing displaces the line parallel to itself. By dropping this assumption, they found that the classical probability regions, which are ellipses, contained only 50% to 80% of the probability claimed. One goal of this year's clinic was to determine the reason for this very large discrepancy. As it turned out, the reason was neither the dropping of the parallel displacement assumption, nor computational errors in the clinic's work, but two equations in the original publication describing the classical approach were printed incorrectly. These errors are probably transcription errors, but no corrections or references to them were found in a search of the relevant literature.

In Section II, the two-sensor problem is described. The parallel displacement assumption is dropped. Based on the assumption that errors of the reported angles are normally distributed, the probability density function of the points of intersection of the computed lines of bearing is given.

In Section III and the Appendix, a re-derivation of the equations of the classical model is carried out and the correct equations for the

probability regions (called Stansfield ellipses) are determined.

In Section IV, it is shown that the Stansfield ellipses as corrected by the clinic, actually contain the claimed probabilities with only very minor differences. However, the densities above and below the location of the emitter are different due to the dropping of the parallel displacement assumption. The contour maps shown in figure 5 show this clearly.

In Sections V and VI, two new probability regions are developed, the "Clinic region" and the "Image region". These are attempts at determining probability regions which contain the same probability as a Stansfield ellipse, but whose areas are smaller than the area of the ellipse.

In Section VII, the Clinic, Image and Stansfield regions are analyzed. It is shown that the Image region is not as "efficient" (larger area for given probability) as the Clinic and Stansfield regions. The Clinic region, on the other hand, is smaller than the Stansfield ellipse for a given level of probability, but the difference is so small that it is hardly worth the effort to determine this much more complicated region. However, the geometric center of the Clinic region moves from below to above the true location of the emitter as the desired probability of the region is increased (see figure 13), while the geometric center of the Stansfield ellipse remains fixed. This result may be of practical value.

In Section VIII, the clinic approaches the three-sensor problem in a manner similar to the two-sensor analysis. The purpose is to find the true density function when the parallel displacement assumption is dropped. Several approaches are taken to obtain a discrete probability density function to approximate the true density function, which is continuous. The different approaches produce very different results. More work should be done in this area.

Section IX is very different from the other sections. Here, a model for a single, active sensor problem is developed. An active sensor measures both direction and distance, taking readings from two different locations. Under the assumption that the systematic errors (direction and distance) are the only significant errors, a scheme to determine the true location of the emitter is presented.

II THE TWO-SENSOR PROBLEM

Given an object or emitter of unknown position, we want to determine its location using a number of sensors. We begin with the two-sensor case. The emitter is located at the intersection of the two lines of bearing determined by the two angles of bearing α_0 and β_0 as shown in figure 1 at the end of the report.

We assume the sensors may report false readings and the goal is to determine a confidence region for the location of the emitter. Towards this end, the clinic considered the related problem of finding a region which contains the point of intersection of the lines of bearing with a specified amount of probability, given that the true location of the emitter is known.

Our assumption is that given the true location of an emitter, the readings the sensors return are random variables, A and B, distributed normally with means equal to the true angles of bearing, and variances σ_A^2 and σ_B^2. We assume the two sensors are independent, so we have the result that the pair of readings has the bivariate normal distribution. Hence, the probability density function for (A,B) is

$$f(\alpha,\beta) = \frac{1}{2\pi\sigma_A\sigma_B} \exp\left[-\tfrac{1}{2}\left(\frac{(\alpha-\alpha_0)^2}{\sigma_A^2} + \frac{(\beta-\beta_0)^2}{\sigma_B^2}\right)\right] \qquad (1)$$

where the values of the random variables A and B are denoted by α and β, and α_0 and β_0 are the true angles of bearing.

However, the location of the emitter is to be given as a point in the x,y plane, and the random variables are in the α,β plane (see figure 2). The mapping of a point from the α,β plane to the x,y plane is given by (next page)

$$x = \frac{D \cdot \tan(\beta)}{\tan(\beta) - \tan(\alpha)}$$
$$y = \frac{D \cdot \tan(\alpha)\tan(\beta)}{\tan(\beta) - \tan(\alpha)} \qquad (2)$$

Since the reported angles of bearing are random variables, and each pair of reported angles uniquely describes a point in the x,y plane, we can transform the density from the α,β plane to a density in the x,y plane. We assume the joint density of A and B is given by equation (1), $f(\alpha,\beta)$. We define two new random variables X and Y as functions of A and B:

$$X = \frac{D \cdot \tan(B)}{\tan(B) - \tan(A)}$$
$$Y = \frac{D \cdot \tan(A)\tan(B)}{\tan(B) - \tan(A)} \qquad (3)$$

Equivalently, A and B can be written as functions of X and Y

$$A = \text{Arctan}[Y/X]$$
$$B = \text{Arctan}[Y/(X-D)] \qquad (4)$$

The joint density of X and Y is then simply

$$g(x,y) = f\{\text{Arctan}[y/x],\text{Arctan}[y/(x-D)]\} \cdot |J| \qquad (5)$$

where $|J|$ is the absolute value of the Jacobian

$$J = \begin{vmatrix} \frac{\delta\alpha}{\delta x} & \frac{\delta\alpha}{\delta y} \\ \frac{\delta\beta}{\delta x} & \frac{\delta\beta}{\delta y} \end{vmatrix} \qquad (6)$$

The density is then

$$g(x,y) = \frac{1}{2\pi\sigma_A\sigma_B} \cdot \left| \frac{y \cdot D}{(x^2+y^2)[(x-D)^2+y^2]} \right| \cdot \qquad (7)$$
$$\exp\left[-\tfrac{1}{2}\left(\frac{[\text{Arctan}(y/x)-\text{Arctan}(y_0/x_0)]^2}{\sigma_A^2} + \frac{[\text{Arctan}(y/(x-D))-\text{Arctan}(y_0/(x_0-D))]^2}{\sigma_B^2}\right)\right]$$

where (x_o, y_o) is the intersection of the lines of bearing. It corresponds to the point (α_o, β_o).

Undoubtedly, this density function makes meaningful analysis difficult. Therefore some other attack is called for. In the following sections, we will describe and compare different approaches to the two-sensor problem. This will include the classical method devised by R.G. Stansfield, and numerical techniques devised by the clinic.

III CLASSICAL APPROACH

Last year's clinic reported that the classical approach to finding probability regions yielded ellipses which contained only approximately 50% to 80% of the probability claimed. Because of the magnitude of this discrepancy, we checked this method to see if the previous clinic had made an error. We also needed to understand the classical approach so that we could compare it to other methods of analysis.

The classical approach was developed primarily by R.G. Stansfield during World War II and published in 1947 (reference 1). Because of the complexity of the density function (7), and because he obviously did not have access to computers, Stansfield made a simplifying assumption of parallel displacement of lines of bearing. This assumption translates angular error to distance error and allows the problem to be modelled using a bivariate normal distribution.

His measure of error is the distance from the true location of the emitter (or target) to the reported line of bearing. It is defined as the length of a line segment perpendicular to the true line of bearing that meets the reported line of bearing (see figure 3). This distance is labeled P1. The distance from the true location of the emitter to the sensor is D1, and the angular error is ψ.

The standard deviation in Stansfield's work is estimated using the fact that for small angles $\sin(\psi)$ is approximately equal to ψ. Also, the distance D1 can be estimated with reasonable accuracy by the distance D1' (see figure 3). By the simple trigonometry of the model, we know that

$$P1 = D1 \times \sin(\psi) \tag{8}$$

which can be estimated as

$$P1 = D1' \times \psi \tag{9}$$

Stansfield's standard deviation is then the distance D1' times the standard deviation of the angular reading (in radians).

To carry this model to the two-sensor case, errors P1 and P2 will be associated with each of the two sensors. Stansfield assumes that these distance errors are independent and that each error can be modeled as a normal probability distribution about a mean of 0 and a standard deviation described above. Therefore, we have a joint normal probability distribution with the random variables P1 and P2. The density function is

$$f(p1,p2) = \frac{1}{2\pi\sigma_1\sigma_2} \exp\left[-\tfrac{1}{2}\left(\frac{p1^2}{\sigma_1^2} + \frac{p2^2}{\sigma_2^2}\right)\right] \tag{10}$$

We now need this distribution written in terms of points rather than the distances P1 and P2. Here, Stansfield makes use of his assumption of parallel displacement of the lines of bearing. With the distance measurements P1 and P2, there is associated a unique parallelogram with one vertex at the true location of the emitter (see figure 4). For each pair of distances, there is also a unique point which is the vertex opposite the true location. Hence, the distances can be converted into points with (x,y) coordinates (see figure 4). Again, making use of the trigonometry of the model, we can rewrite P1 and P2 in terms of the opposite vertex points (x,y).

$$\begin{aligned} P1 &= -x\sin\alpha + y\cos\alpha \\ P2 &= -x\sin\beta + y\cos\beta \end{aligned} \tag{11}$$

With this conversion formula, Stansfield transforms the bivariate normal density, replacing P1 and P2 and multiplying by the appropriate Jacobian determinant. The exponential term

$$\frac{p1^2}{\sigma_1^2} + \frac{p2^2}{\sigma_2^2}$$

thus becomes

$$\frac{1}{\sigma_1^2}[(-\sin\alpha)x + (\cos\alpha)y]^2 + \frac{1}{\sigma_2^2}[(-\sin\beta)x + (\cos\beta)y]^2$$

This can be more easily handled by setting

$$\begin{aligned}\lambda &= \frac{\sin^2\alpha}{\sigma_1^2} + \frac{\sin^2\beta}{\sigma_2^2} \\ \nu &= \frac{\sin\alpha\cos\alpha}{\sigma_1^2} + \frac{\sin\beta\cos\beta}{\sigma_2^2} \\ \mu &= \frac{\cos^2\alpha}{\sigma_1^2} + \frac{\cos^2\beta}{\sigma_2^2}\end{aligned} \tag{12}$$

so that the exponential term can now be written as

$$\lambda x^2 - 2\nu xy + \mu y^2$$

The Jacobian determinant may also be simplified and written as

$$\sqrt{\lambda\mu - \nu^2}$$

Having completed the transformation from distance measures to points, the joint normal density now looks like

$$g(x,y) = \frac{\sqrt{\lambda\mu - \nu^2}}{2\pi} \exp[-\tfrac{1}{2}(\lambda x^2 - 2\nu xy + \mu y^2)] \tag{13}$$

This probability density can be put into a more convenient form by a rotation of axes to eliminate the 'xy' term. Setting

$$\tan(2\emptyset) = \frac{-2\nu}{\lambda - \mu} \tag{14}$$

the rotation is given by

$$\begin{aligned}x &= x'\cos\emptyset - y'\sin\emptyset \\ y &= x'\sin\emptyset + y'\cos\emptyset\end{aligned} \tag{15}$$

Note: where Stansfield uses capital X and Y, we are using x' and y' to avoid confusion between random variables (X and Y) and variables denoting a

rotation of axes.

If these values for x and y are substituted back into the original equation, the result is

$$\lambda x^2 - 2\nu xy + \mu y^2 = \frac{1}{a^2}x'^2 + \frac{1}{b^2}y'^2 \tag{16}$$

where

$$\begin{aligned} \frac{1}{a^2} &= \lambda\cos^2\emptyset - 2\nu\cos\emptyset\,\sin\emptyset + \mu\sin^2\emptyset \\ \frac{1}{b^2} &= \lambda\sin^2\emptyset + 2\nu\cos\emptyset\,\sin\emptyset + \mu\cos^2\emptyset \end{aligned} \tag{17}$$

At this point in Stansfield's derivation, an error appears in the original publication. Please see the appendix for a discussion of the error.

For this transformation, which was unaffected by the error, the Jacobian determinant conveniently reduces to 1. Thus, after two transformations, one to switch from distances to points, and another to rotate axes, we wind up with a joint normal probability distribution with respect to x',y' coordinates, whose density is given by

$$h(x',y') = \frac{\sqrt{\lambda\mu - \nu^2}}{2\pi}\exp\left[-\tfrac{1}{2}\left(\frac{1}{a^2}x'^2 + \frac{1}{b^2}y'^2\right)\right] \tag{18}$$

Stansfield's assumption of parallel displacement allows him to make these transformations. Without it, there would be no meaningful way to move from the distance errors P1 and P2 to x,y coordinates. The resulting expression is the relatively tractable bivariate normal distribution. In fact, one of the properties of the bivariate normal is that the most efficient probability regions will be perfect ellipses determined by the equation (next page)

$$\frac{1}{a^2}x'^2 + \frac{1}{b^2}y'^2 = -2Ln(1-p) \qquad (19)$$

where p is the level of probability desired.

As noted in the appendix, the formulas for the coefficients a and b above are printed incorrectly in Stansfield's paper. The incorrect version makes the values of a and b larger than they should be. Thus, ellipses generated from the incorrect version would be too small and capture far less probability than claimed. This would explain the discrepancy in last year's results.

IV CLINIC ANALYSIS OF STANSFIELD ELLIPSES

With Stansfield's density (18), the problem of finding a probability region is greatly simplified. For any two angle readings α and β, and a desired level of probability, p, an ellipse can be formed which supposedly contains the point of intersection of the reported lines of bearing with probability p. However, because of the simplifying assumption of parallel displacement, the ellipse will not contain exactly that amount of probability. The clinic therefore tested the accuracy of the Stansfield ellipse as a probability region.

Given a region, R, in the x,y plane, and given a two dimensional density, g(x,y), one can determine how much probability is contained in R by evaluating the integral

$$\int\int_R g(x,y)\, dA$$

The clinic performed the integration letting R be a Stansfield ellipse, and g(x,y) the density given by (7). However, since we could not analytically integrate g(x,y), we used numerical methods on the computer.

To verify the accuracy of the numerical results, the clinic evaluated the double integral using both an existing International Mathematics and Statistics Library (IMSL) subroutine (DBLIN), and a modified Simpson's integration algorithm written by the clinic. The two methods yielded virtually the same results.

By varying the levels of probability over three sets of angle readings with $\sigma = 2.0°$, we consistently found that the amount of probability claimed by Stansfield was very close to the amount actually contained in an ellipse (see table 1 at the end of this section). Any discrepencies were insignificant and may be partially due to numerical approximation error.

However, this conclusion holds only if Stansfield ellipses as corrected by the clinic are used. Ellipses derived directly from Stansfield's paper (reference 1, p. 768, equations (15), (16), and (17)), contain only about 50% to 80% of the probability claimed, which is what last year's clinic concluded.

We then examined the difference between the probability in the top and bottom halves of an ellipse. Under Stansfield's assumption of parallel displacement, the probabilities in the top and bottom halves are equal. However, upon dropping the parallel displacement assumption, we found that the probabilities contained in the top and bottom halves are actually not equal. Instead, the top half consistently captures less probability than the bottom half, although surprisingly, the sum of the two halves come very close to the total probability desired (see table 2).

At higher probability levels, the percentage difference between the top and bottom halves is smaller relative to that of lower levels. To explain this, we examined a contour map of the clinic density, as well as probability bands for the Stansfield ellipse. The contour map (see figure 5) graphically demonstrates that the probability in the lower half is concentrated nearer the center of the ellipse, while the probability in the upper half is more dispersed. As we increase the desired probability level, the rate at which the upper half of the ellipse captures probability increases relative to the rate of the lower half.

We also explored this issue of denser bottom half probabilities by looking at ellipses in terms of eight probability bands of equal width (see figure 6). We consistently found bands close to the center below the location of the emitter to contain more probability than corresponding bands above, while the opposite was true for corresponding bands further away from

the center (see table 3). This indicates that when the Stansfield ellipse is made large enough, most of the additional probability must come from the upper half.

Although Stansfield's parallel displacement approximation is not a strict depiction of reality, his method is a simple way to find a region which contains a desired level of probability. This does not necessarily mean, however, that his regions are the "most efficient", in the sense that they capture the desired level of probability in the smallest possible area. The clinic wanted to find out if it was possible to capture the same amount of probability in smaller regions. Sections V and VI describe regions we examined.

TABLE 1

Angle readings are given as α/β

	80/110		50/60		40/150	
Claimed Prob.	Actual Prob.	% Diff	Actual Prob.	% Diff	Actual Prob.	% Diff
0.25	0.2512	0.46	0.2622	4.89	0.2500	-
0.50	0.5029	0.58	0.5287	5.73	0.5000	-
0.75	0.7504	0.06	0.7452	-0.65	0.7495	-0.07
0.95	0.9396	-1.09	0.8791	-7.46	0.9490	-0.10
0.99	0.9802	-0.99	0.9225	-6.81	0.9897	-0.07

Note: $\sigma = 2.0^{\circ}$ and the distance between sensors is 1000.

TABLE 2

80/110

Claimed Prob.	Top	Bottom	Total	% Diff
0.25	0.1162	0.1350	0.2512	16.24
0.50	0.2279	0.2750	0.5029	20.70
0.75	0.3419	0.4085	0.7504	19.47
0.95	0.4475	0.4921	0.9396	9.96
0.99	0.4788	0.5014	0.9802	4.73

50/60

Claimed Prob.	Top	Bottom	Total	% Diff
0.25	0.1006	0.1616	0.2622	60.57
0.50	0.1903	0.3384	0.5287	77.80
0.75	0.2828	0.4624	0.7452	63.54
0.95	0.3811	0.4980	0.8791	30.69
0.99	0.4220	0.5005	0.9225	18.60

40/150

Claimed Prob.	Top	Bottom	Total	% Diff
0.25	0.1244	0.1256	0.2500	0.94
0.50	0.2480	0.2520	0.5000	1.62
0.75	0.3701	0.3794	0.7495	2.54
0.95	0.4654	0.4836	0.9490	3.91
0.99	0.4838	0.5055	0.9893	4.49

Note: $\sigma = 2.0^\circ$ and the distance between the two sensors is 1000.

TABLE 3

	80/110	50/60	40/150
Top Band	0.01276	0.01855	0.00982
2nd Band	0.05649	0.05355	0.05157
3rd Band	0.15208	0.11777	0.15229
4th Band	0.26707	0.23219	0.27010
5th Band	0.28376	0.33246	0.27993
6th Band	0.16456	0.16390	0.16453
7th Band	0.04578	0.00416	0.05298
Bottom Band	0.00491	0.00000	0.00807
Total Prob.	0.98742	0.92258	0.98929

Note: $\sigma = 1.0^\circ$ for the 80/110 case and 2.0° for the other two cases

V CLINIC REGION

The clinic attempted to find a probability region that was more efficient than the Stansfield ellipse. That is, we wanted to pack as much probability into the smallest area. We hoped to be able to do this when we dropped the parallel displacement assumption. But as we have seen, when we drop this assumption, the resulting probability density function is very complicated. Hence, we attacked the problem using a different method.

We first examined the probability of a sensor returning a reading resulting in a line of bearing inside a specified sector or "fan". In figure 7, the true bearing is α, but we assume the reading sensor 1 returns is a random variable, A, distributed normally with mean α and variance σ_A^2. Hence, we can easily determine $P(a1 \leq A \leq a2)$. It is simply $P(A \leq a2) - P(A \leq a1)$. And since we assume the underlying probability distribution is the normal, we can compute close approximations to these probabilities on the computer.

Next, we did the same for the second sensor, so that we have the probability that sensor 2 returns a reading inside the fan between b1 and b2 (see figure 8), where B is distributed normally with mean β and variance σ_B^2.

The two fans intersect and form a quadrilateral. The probability that the two sensors return readings which intersect inside the quadrilateral is simply the probability that sensor 1 returns a reading inside fan 1 and sensor 2 returns a reading inside fan 2. We assume the two sensors are independent, so to find the probability of the quadrilateral, we multiply the probabilities of the fans.

The next step was to form the 3-σ fans (see figure 9). That is, we found the fan formed by moving $\pm 3\sigma$ degrees from α, and the fan formed by moving $\pm 3\sigma$ degrees from β. The reason we use these 3-σ fans is simple. The

quadrilateral formed by the intersection of these fans contains 99.5% of the total probability. To capture 100%, we would have to examine the entire plane, which is simply not possible. So we only look at a subset of the plane, but we choose a subset such that we lose only 0.5% of the probability.

We broke this quadrilateral up into smaller subquadrilaterals, recording the area and probability of each. As can be seen in figure 10, each subquadrilateral has a different area. That means that while two subquadrilaterals may have the same probability, their densities are different. In other words, the amount of probability they pack into a unit area is different.

We then made a very fine grid of 3600 subquadrilaterals and took those of highest density to form a probability region. Since they were of highest density, they contained the most probability in the smallest area. We made a list of the subquadrilaterals, ordering them from highest density to lowest. We formed a probability region by connecting subquadrilaterals together, starting at the top of the list and moving down until we reached the desired level of probability. The areas of these subquadrilaterals were added together to determine the total area of our probability region. Since every one of the subquadrilaterals in the region was of higher density than the subquadrilaterals outside, we concluded that this was the most efficient probability region.

In plotting our region, rather than finding and drawing possibly hundreds of quadrilaterals linked together, we assigned the probability of a subquadrilateral to its center point. In this way we obtained a list of points to represent the subquadrilaterals. The probability region was then the convex hull of these points.

We defined the center point of a subquadrilateral as the point of intersection of the two lines of bearing that bisect the fans forming the subquadrilateral. The resulting grid of center points could also be considered a discretization of the continuous probability density. This discretization is possible because two lines of bearing will always intersect at a point. When we move to the three-sensor case, however, three lines of bearing virtually never intersect at a point, and a discretization of the density is therefore far more difficult (see section VIII).

VI IMAGE REGION

Another approach the clinic examined was a mapping of the most efficient probability region in the α,β plane to the x,y plane. Our results showed that this approach is not as efficient as the Stansfield and Clinic methods.

Recall that we have assumed that the readings the two sensors return are random variables, A and B, each distributed normally. The joint density of A and B is therefore

$$f(\alpha,\beta) = \frac{1}{2\pi\sigma_A\sigma_B} \exp\left[-\tfrac{1}{2}\left(\frac{(\alpha-\alpha_o)^2}{\sigma_A^2} + \frac{(\beta-\beta_o)^2}{\sigma_B^2}\right)\right] \tag{1}$$

A result of this assumption is that in the α,β plane, the most efficient probability region is an ellipse of the form

$$\frac{(\alpha-\alpha_o)^2}{\sigma_A^2} + \frac{(\beta-\beta_o)^2}{\sigma_B^2} = -2\mathrm{Ln}(1-p) \tag{20}$$

where p is the desired level of probability. We assume $\sigma_A^2 = \sigma_B^2$, which implies the probability region is a circle.

We then found the image of this circle (disc) in the x,y plane (hence the name "Image region"). That is, we had a circle in the α,β plane, and transformed it entirely into the x,y plane using the mapping

$$x = \frac{D\cdot\tan(\beta)}{\tan(\beta) - \tan(\alpha)}$$
$$y = \frac{D\cdot\tan(\alpha)\tan(\beta)}{\tan(\beta) - \tan(\alpha)} \tag{21}$$

This region is very difficult to determine analytically. Therefore, we used an approximation to the Image region.

We found 360 points on the boundary of the circle in the α,β plane and performed a point by point transformation into the x,y plane using formulas

(21). This created a region in the x,y plane that resembles an ellipse. The area of this region was calculated by the vector formula for the area of a polygon:

$$\text{Area} = \tfrac{1}{2}(x_1y_2+x_2y_3+\ldots+x_ny_1 - y_1x_2-y_2x_3-\ldots-y_nx_1) \qquad (22)$$

Since we are approximating the area inside a smooth curve by calculating the area of an inscribed polygon, there will be some error in the calculations, but the following analysis shows that this error is small.

We examined the accuracy of the vector formula (22) in approximating the area of an elliptical region by generating 36 unevenly-spaced points on an ellipse. We then compared the area of the polygon formed by the convex hull of these points using (22) to the area of a true ellipse, which is given by the formula πab where a and b are the lengths of the axes of the ellipse. These points were obtained by mapping equally-spaced points on a circle to an ellipse using Stansfield's transformation (see reference 1, equations 9 and 10).

When we used 36 points, the relative error of the approximation was 0.005. For 360 points, the relative error was 0.00005. Thus, the vector formula for the area of a polygon gives a sufficiently accurate approximation to the true area of the Image region.

VII RESULTS

The following tables give comparisons of the Clinic and Image regions with Stansfield ellipses. In the instances where the Clinic region did not contain exactly the same amount of probability as the Stansfield ellipse, figures for regions capturing slightly more are included. The Image region always contains the same amount of probability as the Stansfield ellipse.

We determined probability regions ranging from 10% to 95% for each of three sets of α/β readings, 80/110, 50/60, and 85/95, for sensors located 1000 units apart. In all cases, the standard deviation is $1^{\circ}=\pi/180$ Rad.

For the tables, the columns are labeled as follows

A: Probability captured in the Stansfield ellipse

B: Probability captured in the Clinic region

C: Area of the Image region

D: Area of the Stansfield ellipse

E: Area of the Clinic region

F: Percentage difference in areas of Clinic region and Stansfield ellipse (1-D/E)

TABLE 4

80/110	A	B	C	D	E	F
10%	0.100	0.100	1,494	1,492	1,485	-0.005
20%	0.200	0.201	3,169	3,161	3,150	-0.003
30%	0.300	0.301	5,072	5,053	5,042	-0.002
40%	0.400	0.401	7,272	7,238	7,238	-
50%	0.501	0.501	9,884	9,821	8,810	-0.001
60%	0.601	0.601	13,083	12,983	12,992	0.001*
70%	0.700	0.701	17,208	17,059	17,077	0.001*
80%	0.800	0.800	23,011	22,805	22,845	0.002*
90%	0.898	0.898	32,843	32,627	32,597	-0.001
95%	0.947	0.947	42,478	42,448	42,132	-0.008

*approximation errors

TABLE 5

50/60	A	B	C	D	E	F
10%	0.101	0.101	25,861	25,549	23,878	-0.070
20%	0.202	0.202	55,470	54,111	51,106	-0.059
30%	0.304	0.304	89,827	86,493	82,509	-0.048
40%	0.406	0.407	130,407	123,874	119,904	-0.033
50%	0.508	0.508	179,325	168,086	164,734	-0.020
60%	0.607	0.608	240,013	222,198	220,215	-0.009
70%	0.704	0.705	318,362	291,961	291,622	-0.001
80%	0.797	0.797	426,177	390,285	389,858	-0.001
90%	0.883	0.883	595,796	558,372	543,290	-0.028
95%	0.926	0.926	744,817	726,459	677,785	-0.072

TABLE 6

85/95	A	B	C	D	E	F
10%	0.101	0.102	38,684	38,219	35,987	-0.062
20%	0.202	0.202	82,967	80,946	76,421	-0.059
30%	0.304	0.304	134,344	129,385	123,621	-0.047
40%	0.406	0.407	195,019	185,304	179,448	-0.033
50%	0.508	0.508	268,154	251,442	246,176	-0.021
60%	0.607	0.608	358,880	332,388	329,836	-0.008
70%	0.704	0.704	476,015	436,746	436,252	-0.001
80%	0.797	0.797	637,237	583,830	583,064	-0.001
90%	0.883	0.883	891,007	835,272	812,860	-0.028
95%	0.926	0.926	1,114,062	1,086,714	1,014,349	-0.071

The Image region was always larger than the Stansfield ellipse, even though it contained the same level of probability. In other words, the Image region was never as efficient as the Stansfield ellipse. Thus we discontinued our analysis of this region.

On the other hand, we see that the Clinic region as described in section V is virtually always smaller than the Stansfield ellipse, even though it contains the same level of probability or more. Hence, we say the clinic region is more efficient.

However, it is only slightly more efficient. The Stansfield ellipse is a simple analytic region easy to compute and draw. The Clinic region is much more difficult and time-consuming to obtain and draw. Since the difference is so small, it is not clear whether the gain in efficiency is worth the trouble.

To examine this issue, we looked at why the Clinic region was more efficient. We feel that because the clinic drops the parallel displacement approximation the Clinic region builds up and the Stansfield ellipse builds out. By that we mean the Clinic region chooses the densest subquadrilaterals to fulfill a desired level of probability. Since we know that the probability is generally denser below the true location of the emitter than above, a Clinic region contains more subquadrilaterals from below for lower levels of probability. For higher levels, it continues to append subquadrilaterals upward after most of the lower ones have been used (see figure 11). Therfore we say the clinic region builds "up".

The Stansfield ellipse, on the other hand, builds "out". For increasing levels of probability, it simply encloses the lower probability levels with larger ellipses and performs no shifting (see figure 12).

As a result, the geometric center points of the Clinic region move

upward for increasing levels of desired probability (see figure 13). In an effort to make the Stansfield ellipse more efficient, we artificially forced it to build up rather than out. We did that by relocating its center to the geometric center of the Clinic region at the particular probability level. We then compared the density of the relocated ellipse to the density of the ellipse when it was centered at the intersection of readings.

The results were insignificant. The Stansfield ellipse did become more efficient but the gain was miniscule. At lower levels of probability we found an increase in efficiency, but at higher levels the densities were nearly equal. However, as we have noted earlier in Section IV, the probability in the upper and lower halves of the Stansfield ellipse is always unequally distributed.

Thus, while the Stansfield ellipse is not the most efficient region, it is probably very close. Also since it is so simple and quick to find and draw the Stansfield ellipse, it is a very useful and good approximation.

VIII THE THREE-SENSOR PROBLEM

The clinic has approached the three-sensor problem in a manner similar to the two-sensor analysis. Our purpose is the same, we want to find out what the true density is when we drop Stansfield's parallel displacement assumption. Our method of analysis was to discretize the continuous probability density by generating point estimates for each set of three angle readings. Then, since there is more than one way to generate point estimates, we examined a number of methods and used them to obtain discrete probability densities in the x,y plane.

In the two-sensor case, two intersecting fans form a quadrilateral. In the three-sensor case, though, three intersecting fans will virtually never form a usable subregion (see figure 14). Therefore, we cannot approximate the continuous density as readily as we did in the two-sensor case. We decided to discretize the density as described in the next paragraph.

We assign all the probability of each of three fans to the lines of bearing bisecting them. We assume the sensors are independent, so the probability of returning a particular set of three readings is the product of the probabilities of the individual readings. The three lines of bearing form a triangle (see figure 15), and we assign all the probability of the set of readings to a point to represent the triangle. There are several ways to determine a reasonable point to use, and we examined a number of possible methods.

Stansfield develops a maximum likelihood estimate, hereafter referred to as the MLE, as a point estimate within a triangle. The derivation of the MLE proceeds from the joint normal density, which Stansfield uses because of his parallel displacement assumption. The principle of maximum likelihood estimation states that for a given set of observations, in this case the

angle readings, we maximize the probability density with respect to the unknown parameters we wish to estimate. Here, our unknown parameters are are the x and y coordinates of the point estimate.

These MLE points have some interesting characteristics. Within the triangle, they are generally located nearest the line of bearing that is closest to the true location of the emitter, and they are farthest from the more acute angles of the triangle. Stansfield mentions this in his paper, and our computer analysis appears to confirm his statement.

We also looked at the "center" of a triangle as a point to represent the triangle. There are, however, a number of ways to define the center of a triangle. The clinic considered five different approaches to determine a point to represent a triangle in the sense that the probability of the set of readings (determining the triangle) is assigned to that point. The approaches or methods were the following.

1) Minimizing the sum of the distances from each vertex to the center

2) Minimizing the sum of the squares of the distances from each vertex to the center

3) Angle bisection

4) Intersection of the medians

5) Perpendicular bisection.

For acute triangles, all the methods gave center points that lay inside the region, while for obtuse triangles, the perpendicular bisection method left us with a center point located outside the triangle. Although there is only a one in four chance that the emitter is inside a triangle formed by any three lines of bearing (see reference 1), the triangle is nonetheless the only bounded region in which to look for the emitter. Therefore, since we wanted ths representative point to lie inside the triangle, we did not

further consider the method of perpendicular bisection. Also, it minimizing sums of squares (method 2) and intersecting the medians (method 4) gave identical results. Thus, we will only discuss methods 1, 2, and 3.

The first method, minimizing the sum of the distances, requires minimizing the function

$$D1(x,y) = \sqrt{(x_1-x)^2 + (y_1-y)^2} + \sqrt{(x_2-x)^2 + (y_2-y)^2} + \sqrt{(x_3-x)^2 + (y_3-y)^2} \tag{23}$$

where (x_1,y_1), (x_2,y_2), and (x_3,y_3) are the vertices of the triangle. Since minimizing D1 by standard calculus methods is extremely complicated, a computer program was written which searched the triangle for the x and y coordinates for which the function D1 was minimized.

The second method, minimizing the sum of squares of the distances, proved to be quite simple. It required minimizing the function

$$D2(x,y) = (x_1-x)^2+(y_1-y)^2 + (x_2-x)^2+(y_2-y)^2 + (x_3-x)^2+(y_3-y)^2 \tag{24}$$

Taking the partial derivatives of D2 with respect to x and y and setting equal to zero yields the point estimate

$$(x,y) = [(x_1+x_2+x_3)/3 \ , \ (y_1+y_2+y_3)/3] \tag{25}$$

The last method is angle bisection. It required finding the intersection of the three lines that bisect the angles of the triangle.

Figure 16 shows where the various methods put the representative point for a particular triangle.

The clinic tested to see how much difference the selection of various representative points would have on the discretization of the probability density.

We created point clouds, associating probabilities with each point. These point clouds were created by varying the lines of bearing from each of

the three sensors by $\frac{1}{2}\sigma$ between $+3\sigma$ and -3σ. Thus, for each sensor, 13 lines of bearing were produced, which in turn created 13^3 or 2197 different triangles. Then, within each triangle, we calculated the representative points.

For purposes of comparison, we analyzed two candidates for the representative point, Stansfield's MLE and the geometric center defined by the sum of squares of the distances. We used the sum of squares method because of its relative ease in programming.

In order to determine a discrete approximation of the continuous density, we first split the area of the plane containing the point cloud into a 40 by 40 grid of rectangles. Within each of the resulting 1600 rectangles, we tabulated the number of points (if any) contained and summed the probabilities associated with each point. This sum of probabilities was then assigned to the rectangle.

To calculate the size of a region at a particular probability level, we summed the rectangles of highest probability until we reached the desired level. The area of the probability region is simply the sum of the areas of the rectangles, which are all of uniform size.

Our results show that the choice of point estimate makes a great deal of difference in the nature of resulting point clouds and in the areas of corresponding probability regions (see figures 17 and 18 for examples of point clouds). The area comparisons (tables 7 and 8) show this clearly.

Note that even though the areas obtained using the MLE points are smaller, it does not necessarily mean that the method provides "best" points to choose for our purposes. It is not certain which discretized density most accurately reflects the true density in the x,y plane.

We would suggest that further work on this problem be directed toward

finding the true density function, as was done in the two-sensor case, by means of a transformation that would map the three angle readings to coordinates in the x,y plane. The formulation of this mapping is still uncertain, since these different point clouds represent competing definitions of the transformation needed, and it is not clear which of these transformations is most appropriate.

TABLE 7
AREA COMPARISONS

Grid region created from MLE points

Angle readings	Level of probability 0.9	0.75	0.5
80,110,69	10689	5984	2813
50,60,41	157759	88239	42782
40,150,-58	1110	600	257
85,95,84	396899	224619	95954

Stansfield ellipses

Angle readings	Level of probability 0.9	0.75	0.5
80,110,69	10877	6594	3274
50,60,41	220152	123544	66272
40,150,-58	1211	729	365
85,95,84	499087	300480	150240

Percentage difference

Angle readings	0.9	0.75	0.5
80,110,69	1.7	9.4	16.4
50,60,41	39.5	50.2	54.9
40,150,-58	9.1	21.5	42.0
85,95,84	25.7	33.8	56.6

In these cases the Stansfield ellipse is LARGER than the corresponding Grid region by the given percentage.

TABLE 8
AREA COMPARISONS

Grid region created from "minimized sum of squares" points (method 2)

Angle readings	Level of probability 0.9	0.75	0.5
80,110,69	20630	11269	4334
50,60,41	455157	273093	136546
85,95,84	3668714	1690094	564417

Stansfield ellipses

Angle readings	Level of probability 0.9	0.75	0.5
80,110,69	10877	6594	3274
50,60,41	220152	132544	66272
85,95,84	499087	300480	150240

Percentage difference

Angle readings	Level of probability 0.9	0.75	0.5
80,110,69	-47.3	-41.5	-24.5
50,60,41	-51.6	-51.5	-51.5
85,95,84	-86.4	-82.2	-73.4

In these cases, the Stansfield ellipse is SMALLER than the corresponding Grid region by the given negative percentages.

IX SYSTEMATIC ERROR

The previous sections of the report discussed random errors in passive sensors. This section examines systematic errors in active sensors. An active sensor reports distance as well as direction.

For this model there is only one sensor, which returns direction and distance readings at point P1 (see figure 19). It is then moved a distance D to point P2, and returns new readings. The two measured direction readings form the angles α and β and the two distance readings originate at P1 and P2 and are labeled D1 and D2.

We assume the readings the sensor returns may be wrong. As an example, in figure 19, it is clear the direction and/or distance readings are off since the readings at point P1 do not agree with the readings at point P2. We assume there are no random errors, but only systmatic errors associated with the sensor which are the same at both locations. That is, if the sensor reports a direction reading which actually deviates by ϵ degrees at point P1, it will report a direction reading deviating by ϵ degrees at point P2. Likewise, how far the distance reading is off at point P1 is how far the distance reading will be off at point P2.

We first examine the directional error, disregarding distance for the moment. In figure 20, we see that if α and β are the true bearings, the emitter will be located at point E. But if the directional error is ϵ, the emitter will be located at point E'. We continue in this fashion, producing a number of points which would indicate the true location of the emitter for several directional errors. We then find the Lagrange polynomial using these generated points. We now have the equation of a curve, somewhere on which the emitter is truly located.

Now we examine distance error. In figure 21, we see that if D1 and D2

are indeed the true distances, then the emitter must be located at either point E or F. But if the distance error is δ, the emitter would be located at either E' or F'. We continue producing points which would indicate the true location of the emitter if the distance error were various given amounts. We assume that in practice some points can be disregarded, such as F and F', because it may be clear the emitter is not located in that direction. We then find the Lagrange polynomial using the generated points. As in the directional error case, we now have the equation of a curve, somewhere on which the emitter is truly located.

So now we say the true location of the emitter is somewhere on curve 1 (figure 22), but also somewhere on curve 2. Therefore, the true location must be at the intersection of these two curves.

APPENDIX

The CGS/CMC Mathematics Clinic discovered an error in the paper by R.G. Stansfield, published in the Journal of the Institution of Electrical Engineering, volume 94, Part IIIA, 1947, under the title "Statistical Theory of D.F. Fixing".

The error is in equations (15) and (16), p. 768, which give the coefficients for the elliptical confidence region in the x,y plane. As they stand now, the equations are

$$(15) \quad \frac{1}{a^2} = 2\lambda - \nu\tan\emptyset$$

$$(16) \quad \frac{1}{b^2} = 2\mu + \nu\tan\emptyset$$

They should be

$$(15) \quad \frac{1}{a^2} = \lambda - \nu\tan\emptyset$$

$$(16) \quad \frac{1}{b^2} = \mu + \nu\tan\emptyset$$

The mathematical derivation of (15) and (16) proceeds as follows. Starting with (11), p. 768,

$$P(x,y)\,dxdy = \frac{1}{2\pi}\sqrt{\lambda\mu - \nu^2}\,\exp[-\tfrac{1}{2}(\lambda x^2 - 2\nu xy + \mu y^2)]\,dxdy$$

Stansfield transforms the density to a system of X,Y coordinates rotated through an angle $\emptyset$, where $\emptyset$ is given by

$$\tan 2\emptyset = \frac{-2\nu}{\lambda - \mu}$$

The transformation is given by (next page)

$$x = X\cos\theta - Y\sin\theta$$

$$y = X\sin\theta + Y\cos\theta$$

This changes $\lambda x^2 - 2\nu xy + \mu y^2$ into $\frac{1}{a^2}X^2 + \frac{1}{b^2}Y^2$ where

$$\frac{1}{a^2} = \lambda\cos^2\theta - 2\nu\cos\theta\sin\theta + \mu\sin^2\theta$$

$$\frac{1}{b^2} = \lambda\sin^2\theta + 2\nu\cos\theta\sin\theta + \mu\cos^2\theta$$

By the definition of tan 2θ, we know that

$$\mu = \lambda + \frac{2\nu}{\tan 2\theta}$$

so that $$\frac{1}{a^2} = \lambda\cos^2\theta + (\lambda + \frac{2\nu}{\tan 2\theta})\sin^2\theta - 2\nu\cos\theta\sin\theta$$

$$= \lambda(\cos^2\theta + \sin^2\theta) + \nu\sin\theta(\frac{2}{\tan 2\theta}\sin\theta - 2\cos\theta)$$

$$= \lambda + \nu\sin\theta(\frac{1 - \tan^2\theta}{\tan\theta}\sin\theta - 2\cos\theta)$$

since $\tan 2\theta = \frac{2\tan\theta}{1 - \tan^2\theta}$. Continuing

$$\frac{1}{a^2} = \lambda + \nu\sin\theta[(1-\tan^2\theta)(\frac{\cos\theta}{\sin\theta})\sin\theta - 2\cos\theta]$$

$$= \lambda + \nu\sin\theta[\cos\theta(1 - \tan^2\theta - 2)]$$

$$= \lambda + \nu\sin\theta[-\cos\theta(\tan^2\theta + 1)]$$

$$= \lambda - \nu\sin\theta(\cos\theta\sec^2\theta)$$

$$= \lambda - \nu\sin\theta(\cos\theta\frac{1}{\cos^2\theta})$$

$$= \lambda - \nu\tan\theta$$

The computations for $\frac{1}{b^2}$ proceed almost identically, except we replace λ instead of μ

$$\lambda = \mu - \frac{2\nu}{\tan 2\emptyset} .$$

So
$$\frac{1}{b^2} = (\mu - \frac{2\nu}{\tan 2\emptyset})\sin^2\emptyset + \mu\cos^2\emptyset + 2\cos\emptyset\sin\emptyset$$

$$= \mu(\cos^2\emptyset + \sin^2\emptyset) - \nu\sin\emptyset(\frac{2}{\tan 2\emptyset}\sin\emptyset - 2\cos\emptyset)$$

$$= \mu - \nu\sin\emptyset(\frac{1 - \tan^2\emptyset}{\tan\emptyset}\sin\emptyset - 2\cos\emptyset)$$

since $\tan 2\emptyset = \frac{1 - \tan^2\emptyset}{2\tan\emptyset}$. Continuing

$$\frac{1}{b^2} = \mu - \nu\sin\emptyset[(1 - \tan^2\emptyset)\cos\emptyset - 2\cos\emptyset]$$

$$= \mu - \nu\sin\emptyset\cos\emptyset(-\tan^2\emptyset - 1)$$

$$= \mu + \nu\sin\emptyset\cos\emptyset\sec^2\emptyset$$

$$= \mu + \nu\tan\emptyset$$

Therefore, we assert that equations (15) and (16) should be

$$(15) \quad \frac{1}{a^2} = \lambda - \nu\tan\emptyset$$

$$(16) \quad \frac{1}{b^2} = \mu + \nu\tan\emptyset$$

FIGURE 1

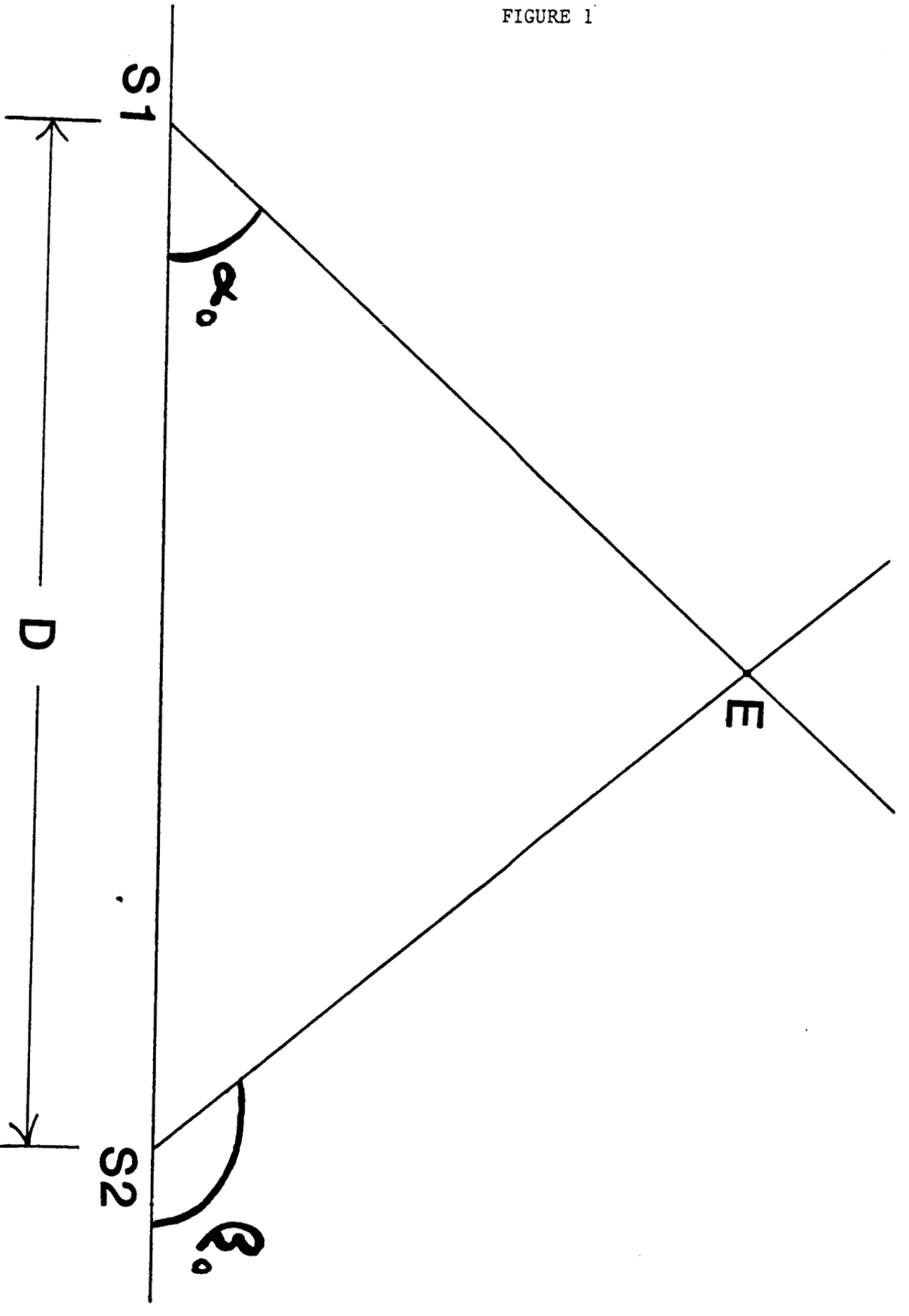

FIGURE 2

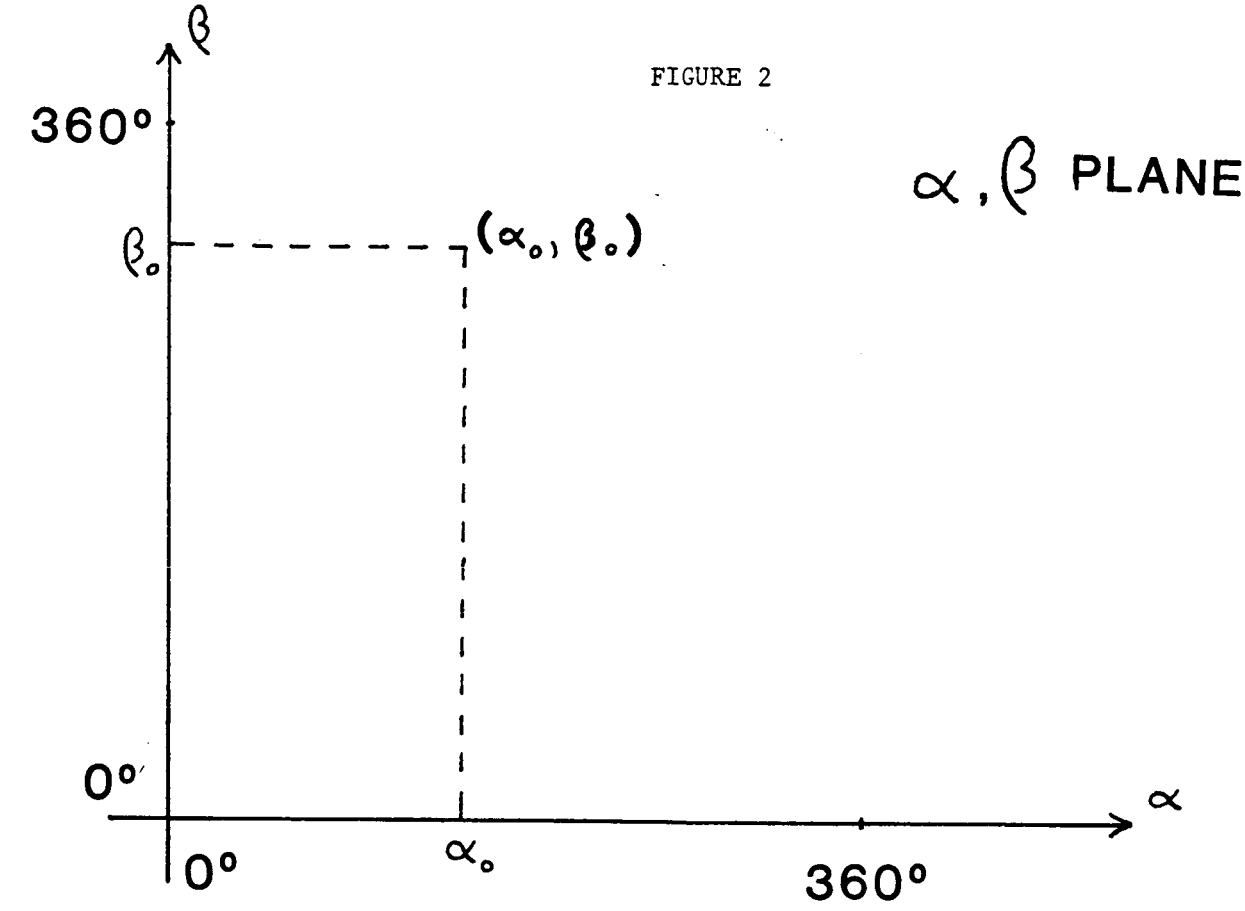
β
360°
β₀
(α₀, β₀)
0°
α
0°
α₀
360°
α, β PLANE

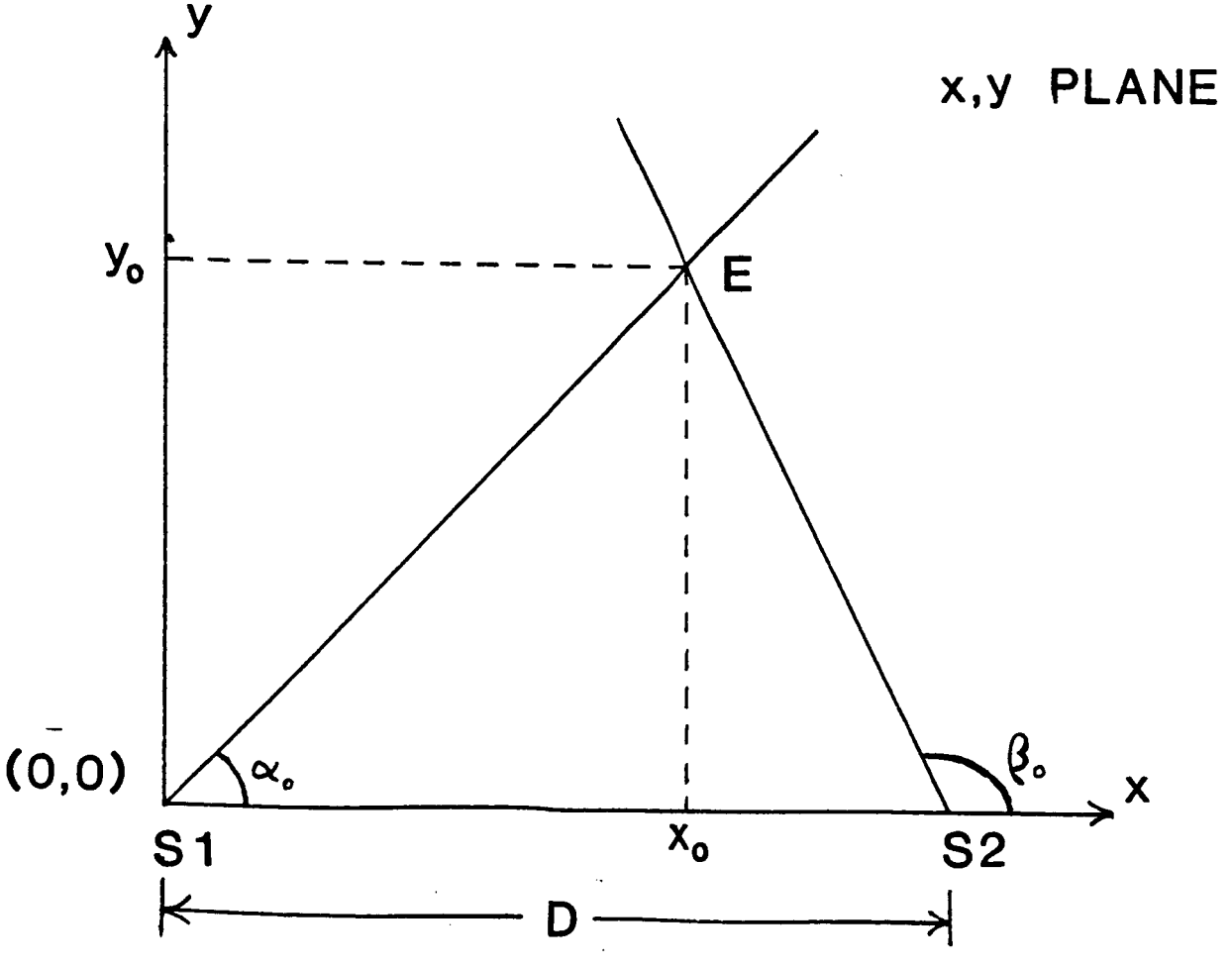
y
y₀
E
(0,0)
α₀
β₀
x
S1
x₀
S2
D
x,y PLANE

FIGURE 3

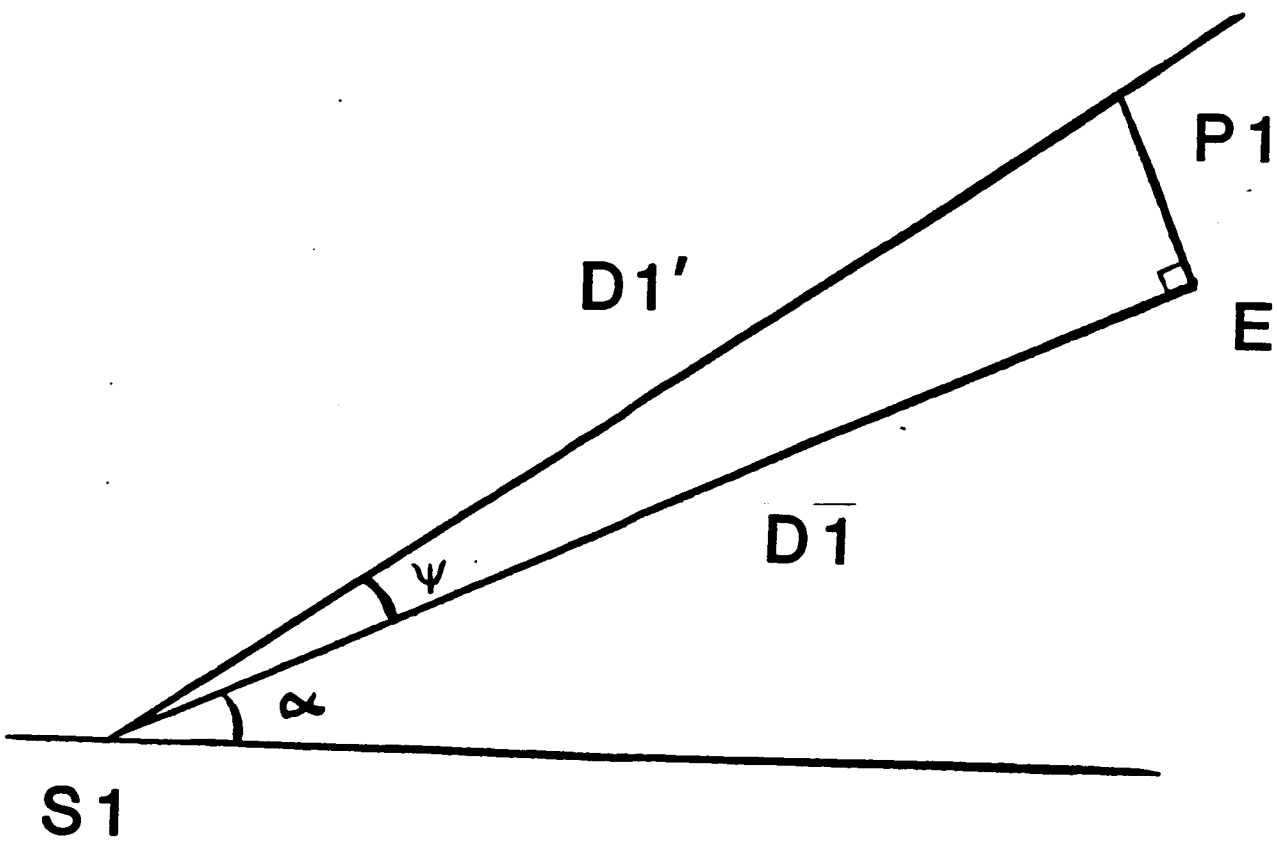

FIGURE 4

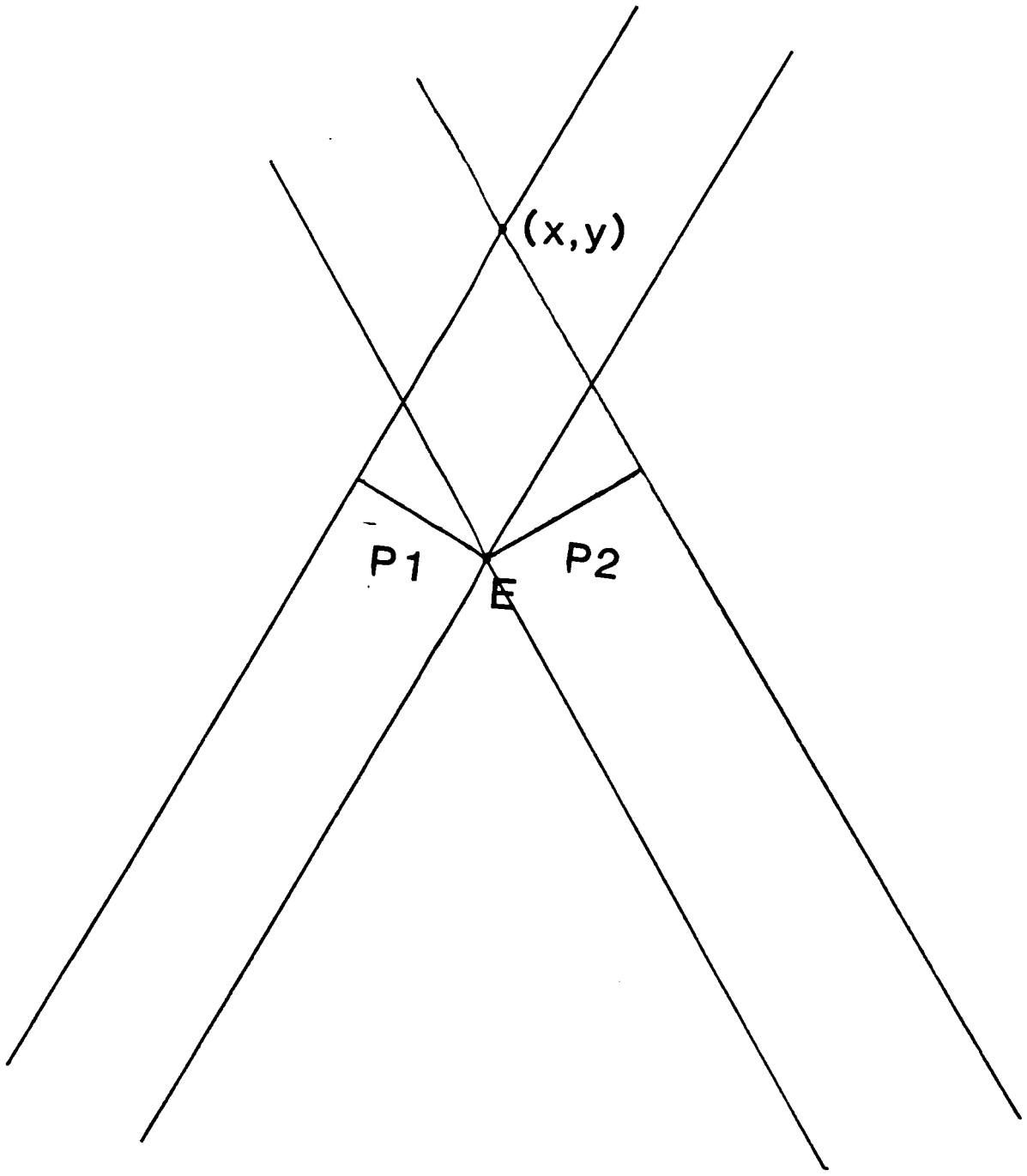

FIGURE 5

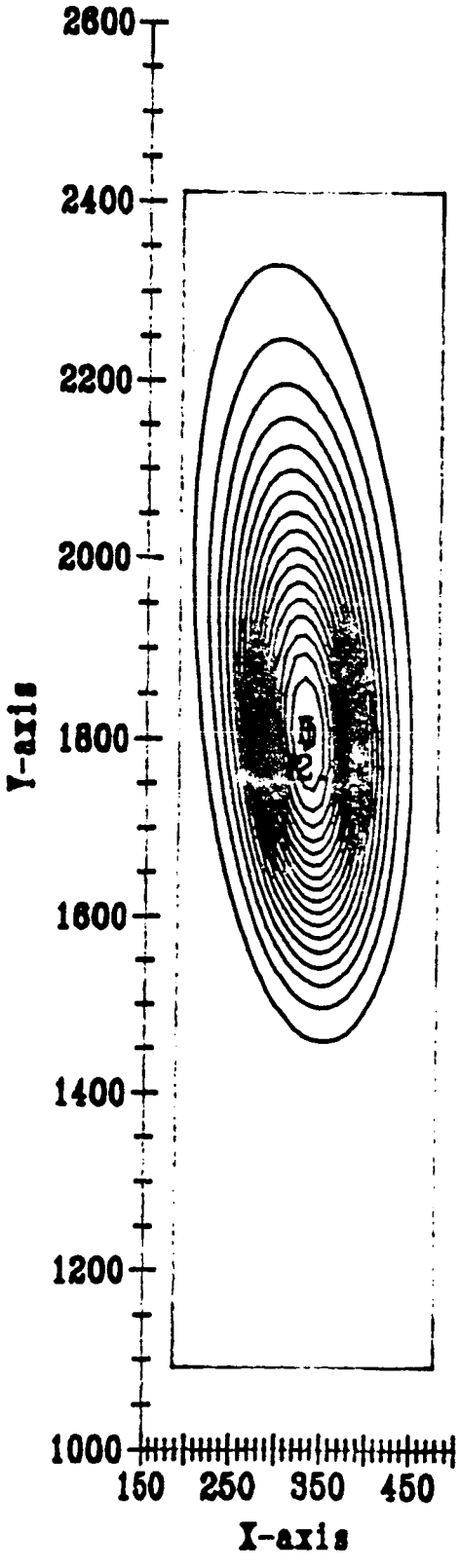
2600
2400
2200
2000
1800
1600
1400
1200
1000
Y-axis
150
250
350
450
X-axis

FIGURE 6

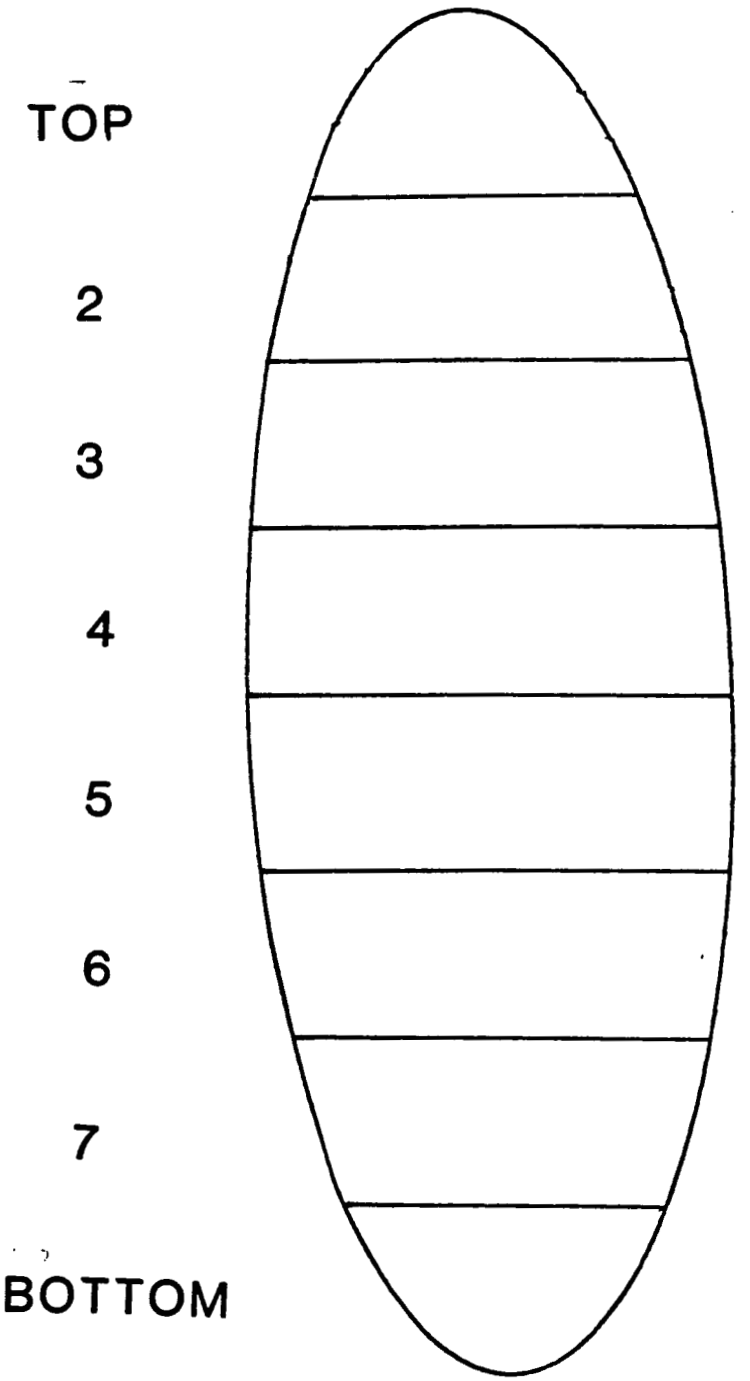

FIGURE 7

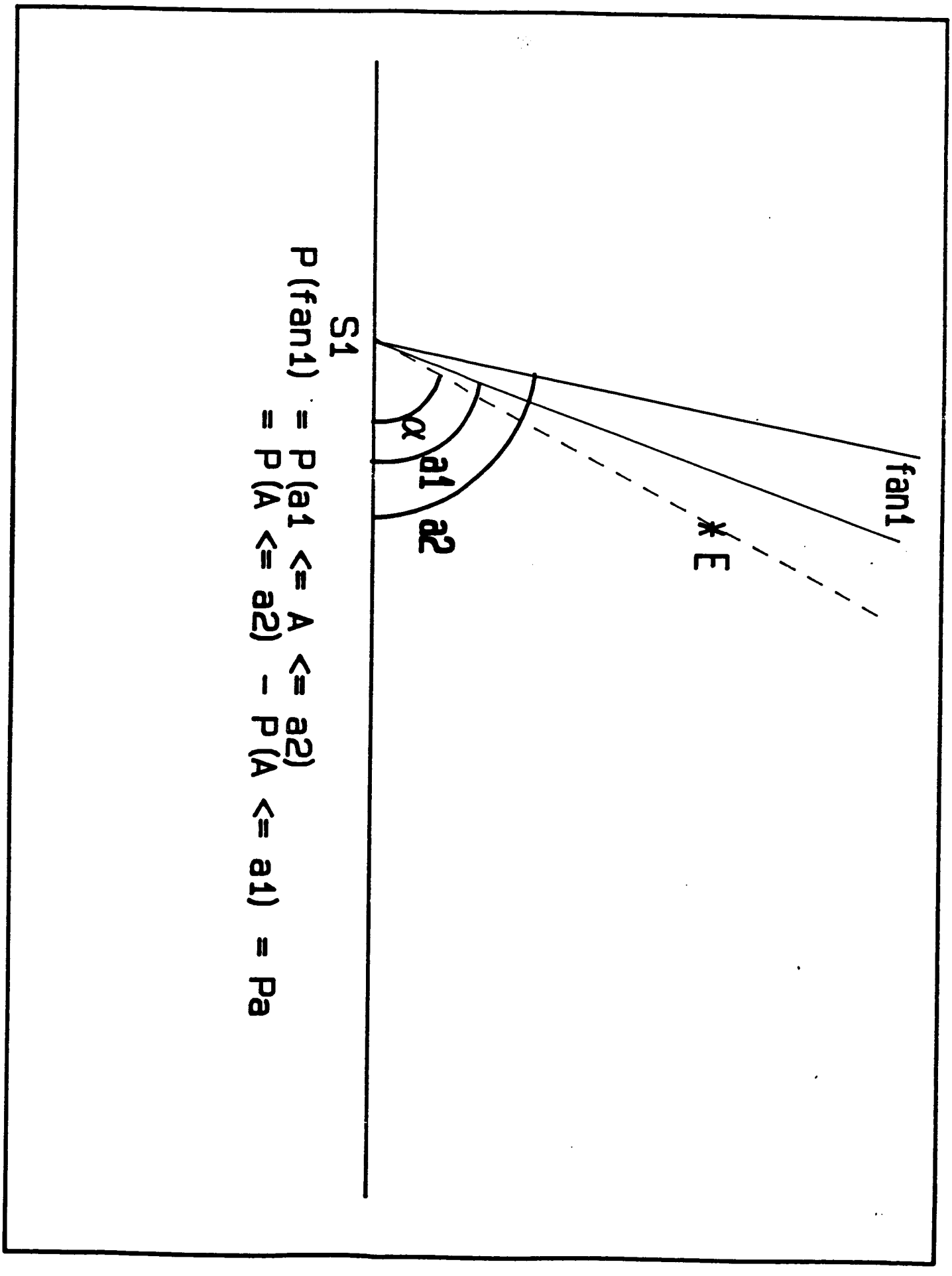

FIGURE 8

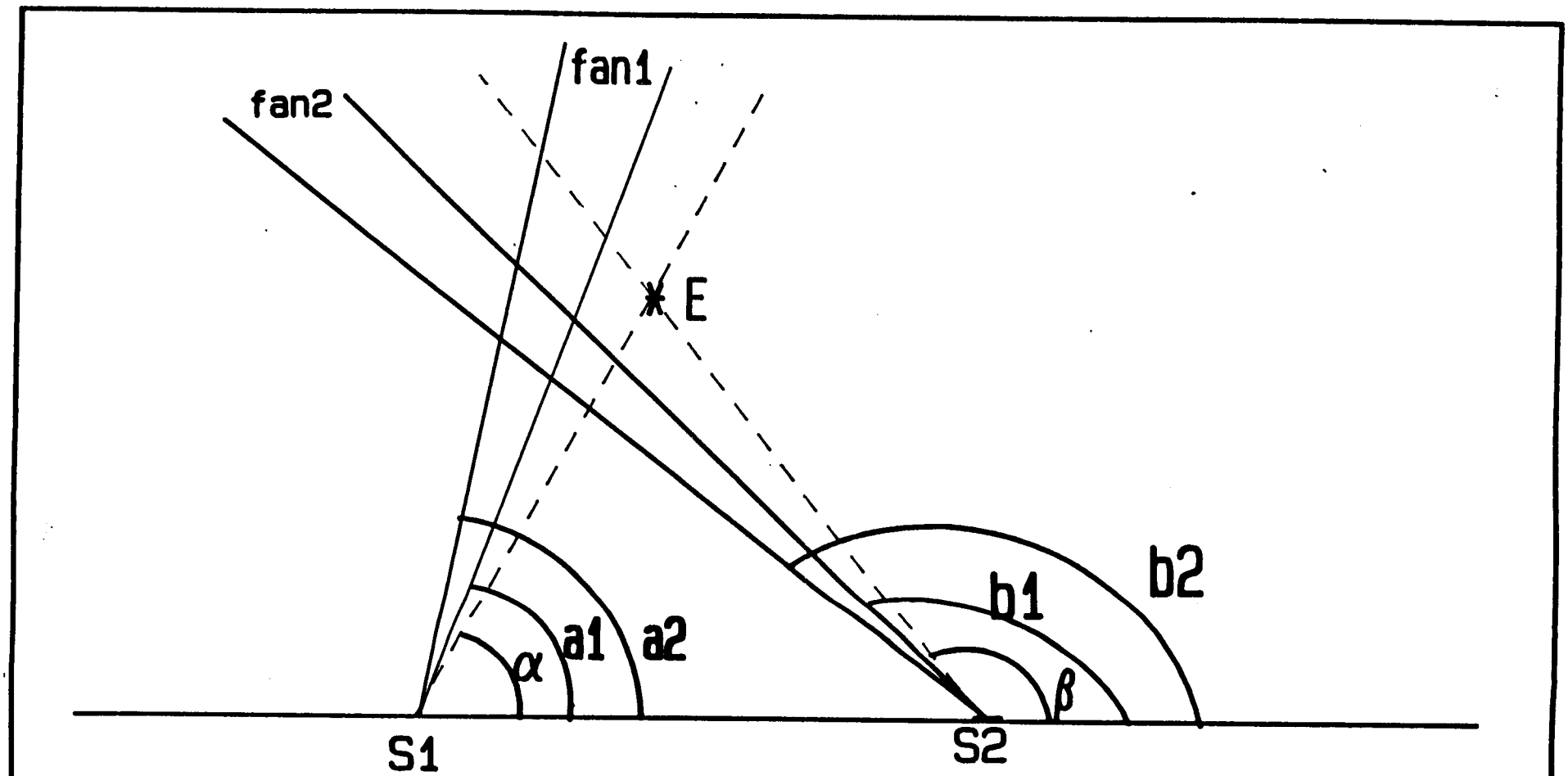

$$P(\text{fan1}) = P(a1 \le A \le a2) = P(A \le a2) - P(A \le a1) = Pa$$

$$P(\text{fan2}) = P(b1 \le B \le b2) = P(B \le b2) - P(B \le b1) = Pb$$

$$P(\text{quad}) = Pa \times Pb$$

FIGURE 9

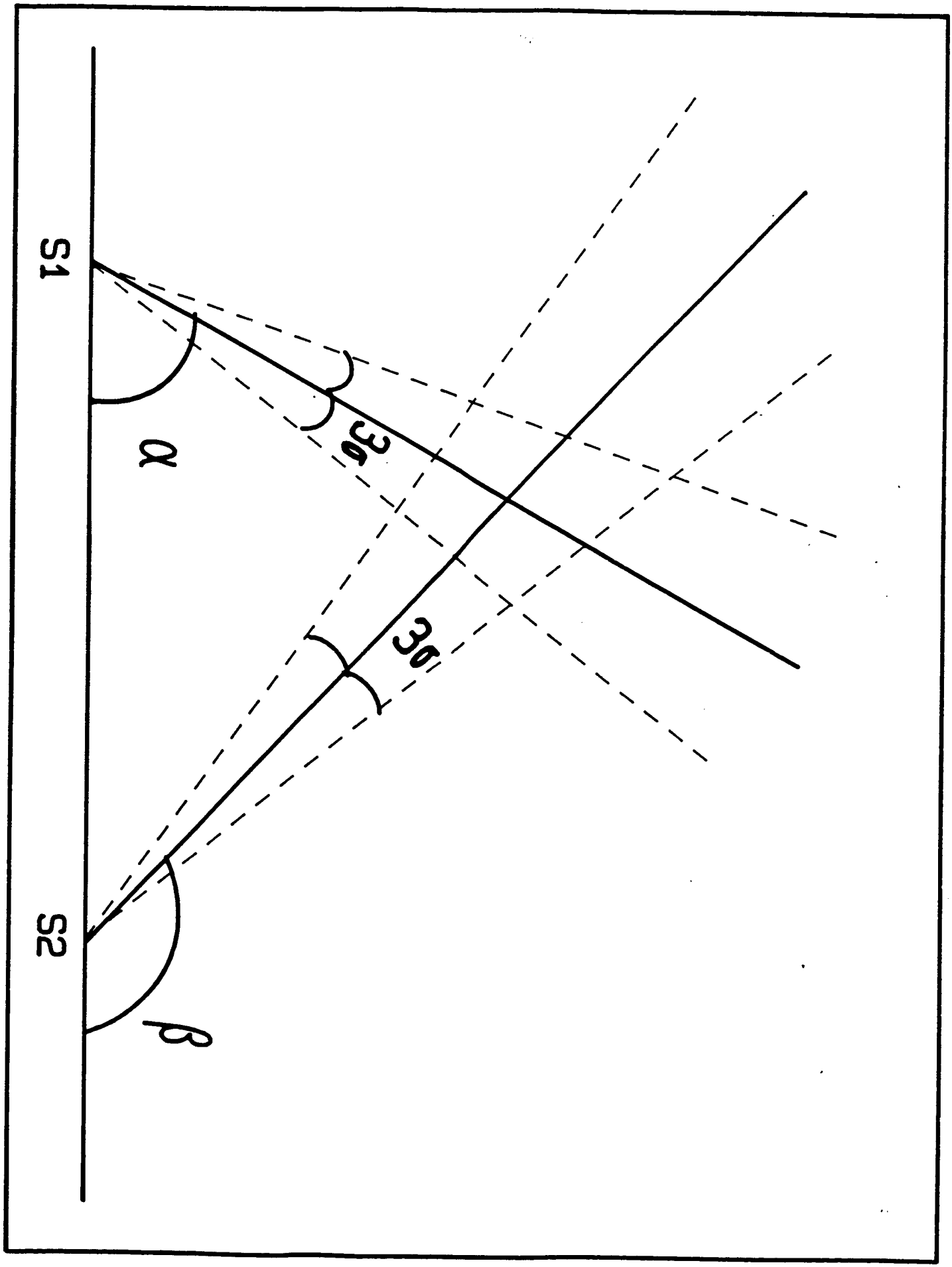

FIGURE 10

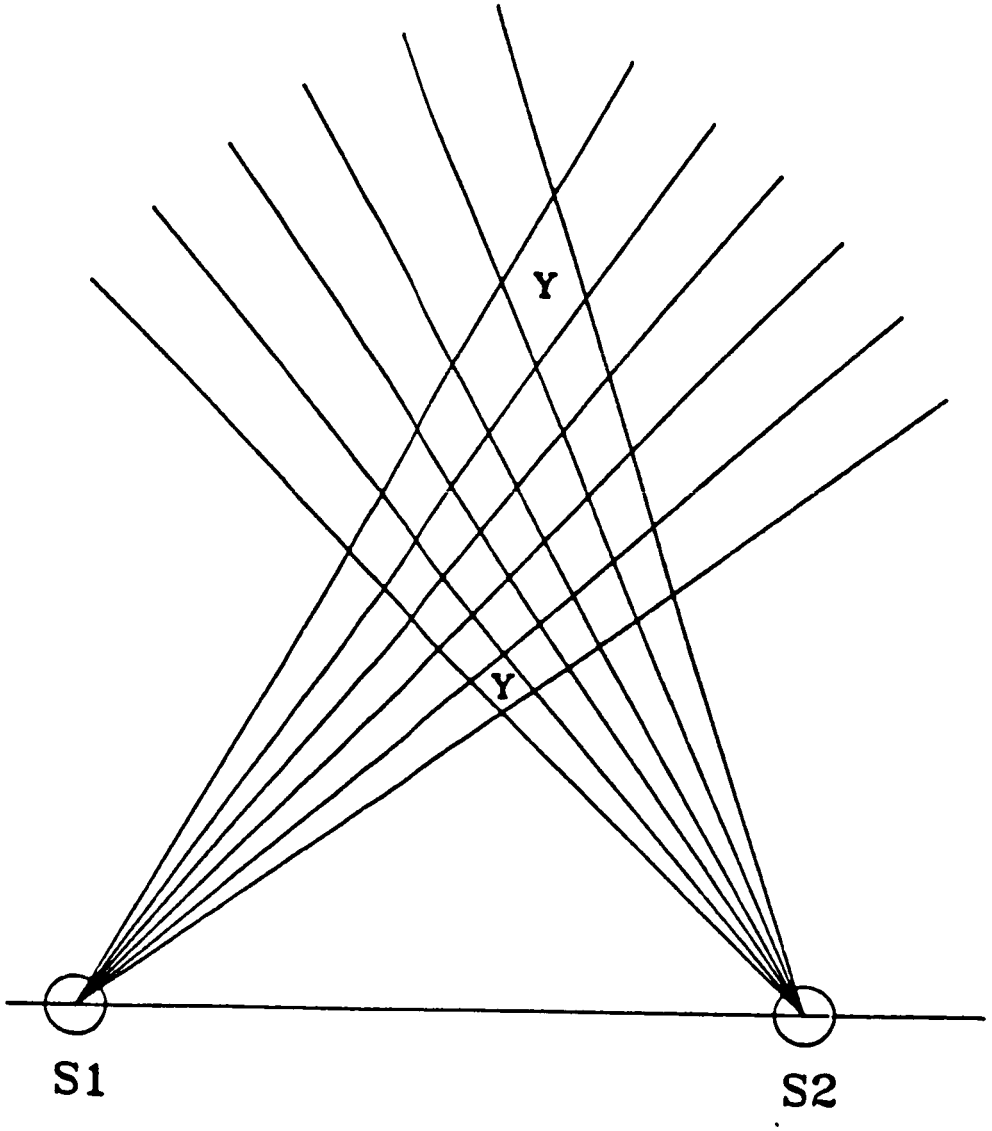

FIGURE 11

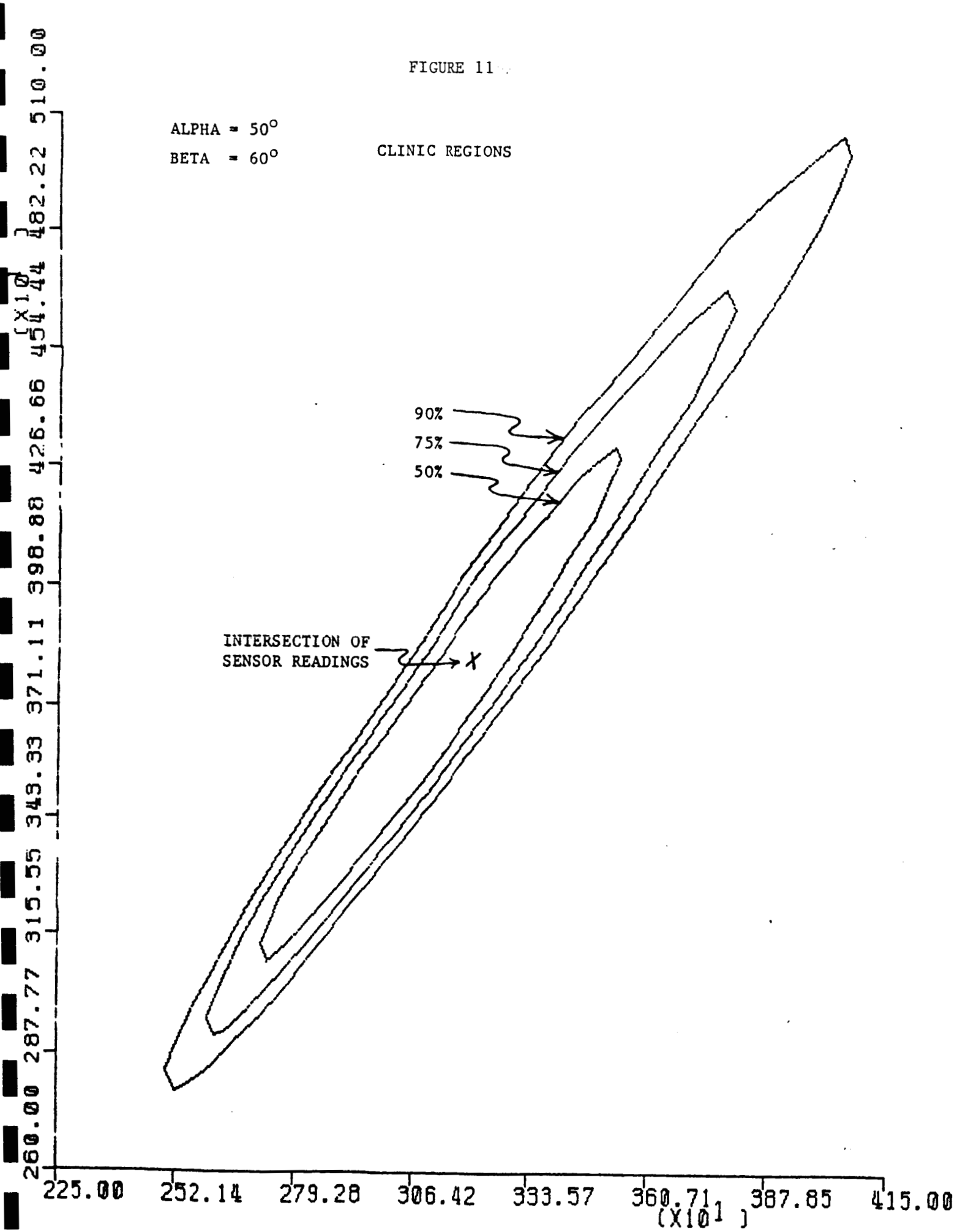
ALPHA = 50°
BETA = 60°
CLINIC REGIONS
90%
75%
50%
INTERSECTION OF
SENSOR READINGS
260.00
287.77
315.55
343.33
371.11
398.88
426.66
454.44
482.22
510.00
(X10)
225.00
252.14
279.28
306.42
333.57
360.71
387.85
415.00
(X10)

FIGURE 12

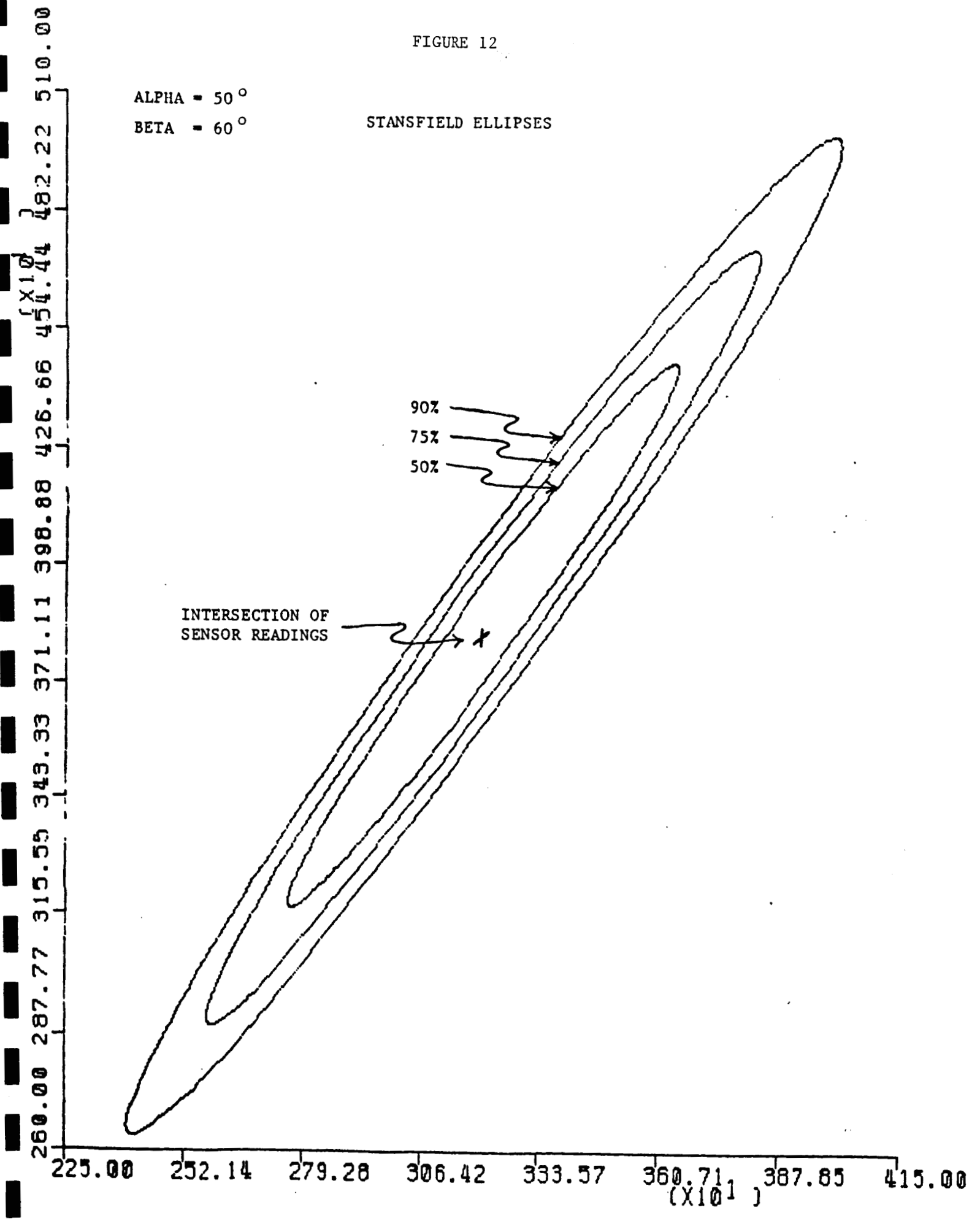
ALPHA = 50°
BETA = 60°
STANSFIELD ELLIPSES
90%
75%
50%
INTERSECTION OF
SENSOR READINGS
260.00
287.77
315.55
343.33
371.11
398.88
426.66
454.44
482.22
510.00
(X10)
225.00
252.14
279.28
306.42
333.57
360.71
387.85
415.00
(X10)

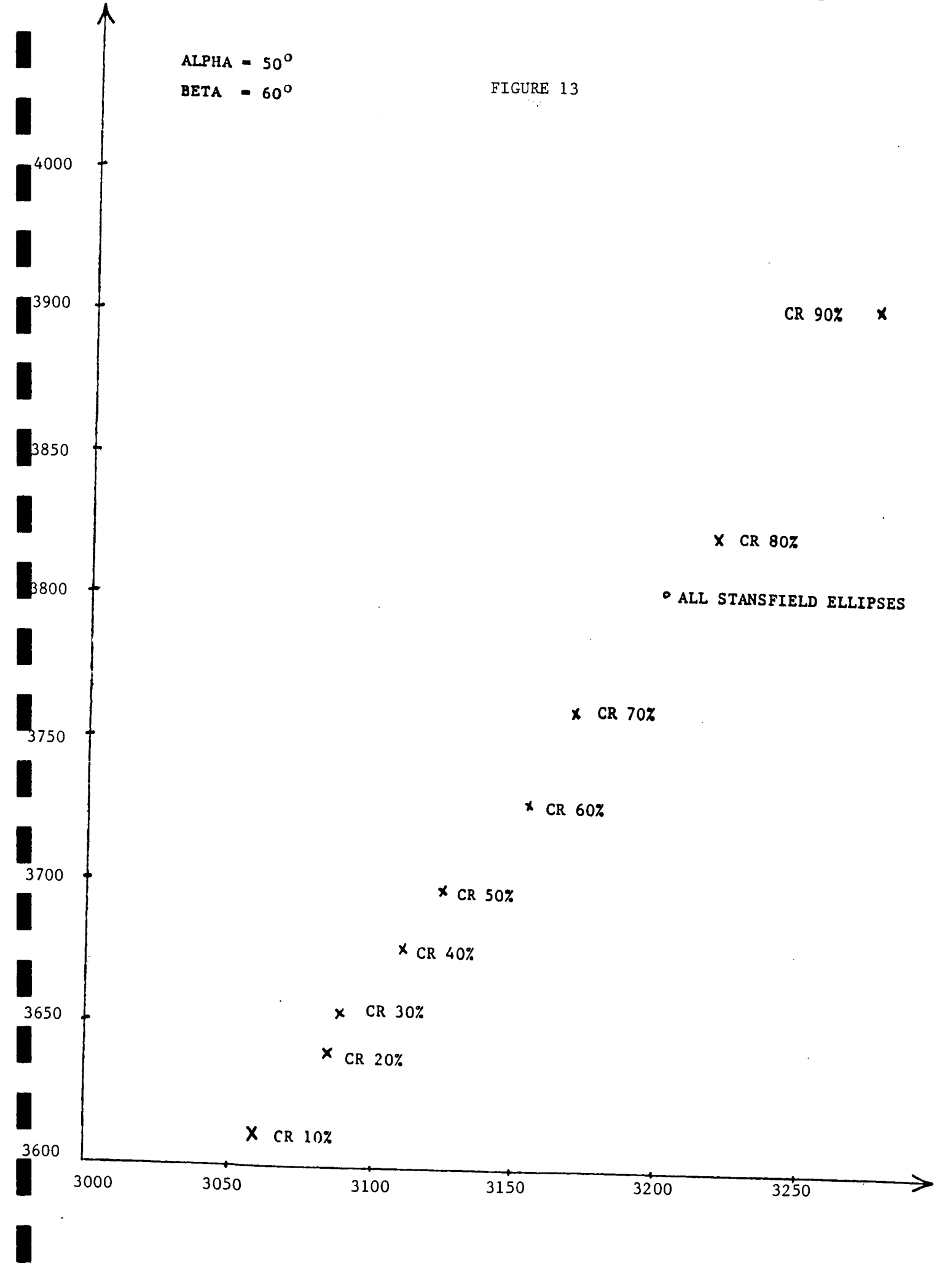
ALPHA = 50°
BETA = 60°
4000
3900
3850
3800
3750
3700
3650
3600
3000
3050
3100
3150
3200
3250
CR 90%
CR 80%
ALL STANSFIELD ELLIPSES
CR 70%
CR 60%
CR 50%
CR 40%
CR 30%
CR 20%
CR 10%

FIGURE 13

FIGURE 14

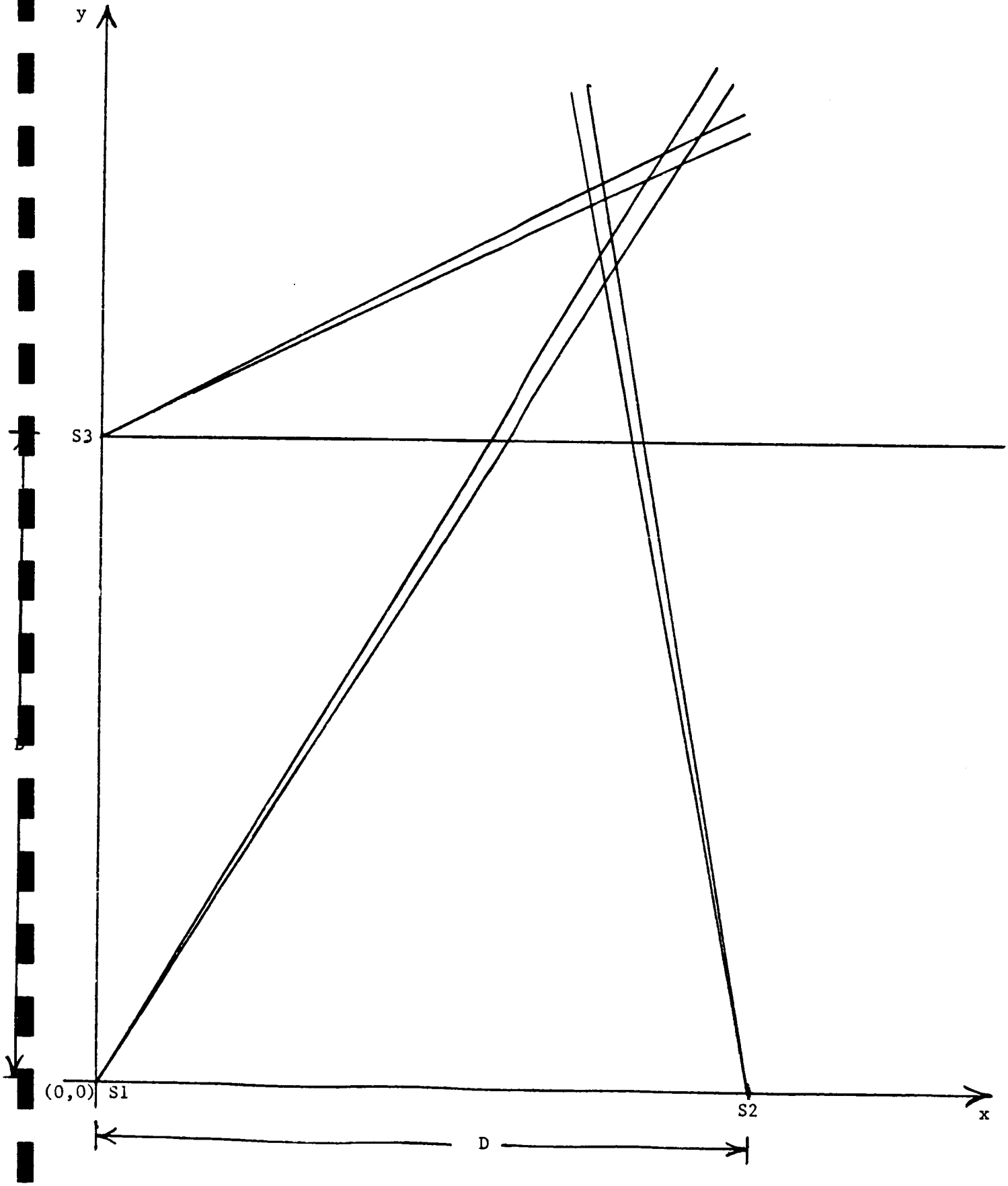

FIGURE 15

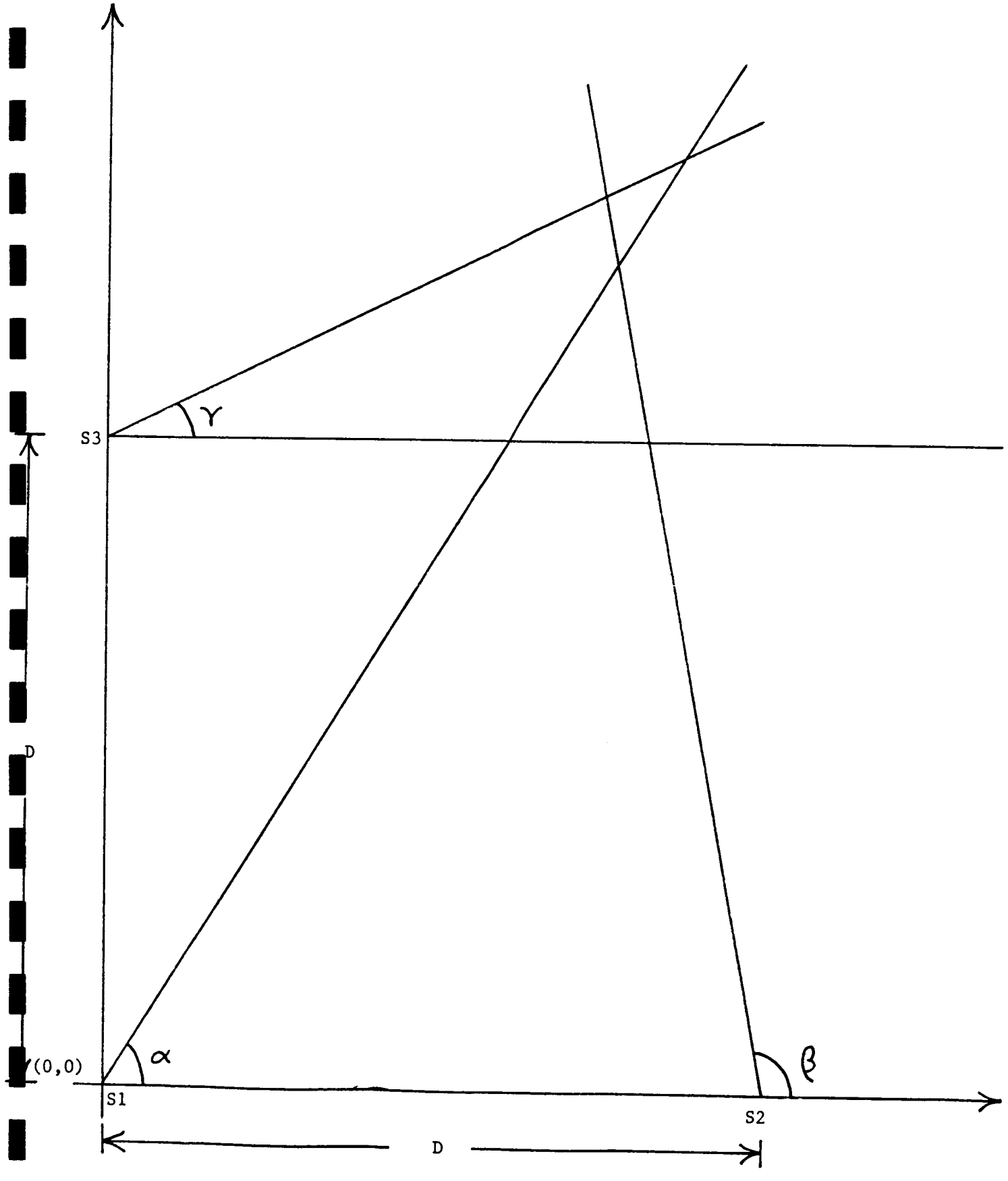

FIGURE 16

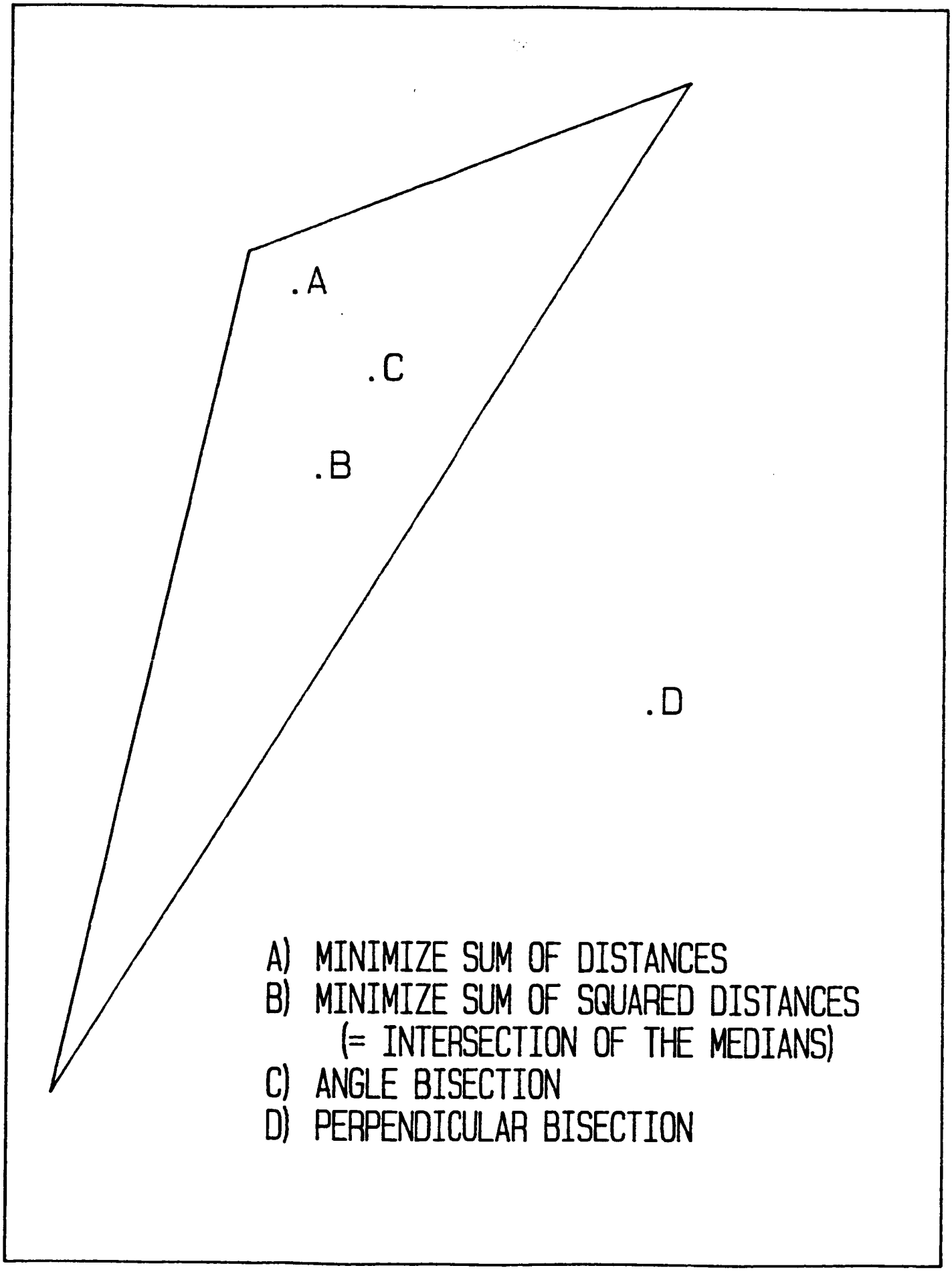
.A
.C
.B
.D
A) MINIMIZE SUM OF DISTANCES
B) MINIMIZE SUM OF SQUARED DISTANCES
(= INTERSECTION OF THE MEDIANS)
C) ANGLE BISECTION
D) PERPENDICULAR BISECTION

FIGURE 17

260.00 288.57 317.14 345.71 374.28 402.85 431.42 460.00 488.
[X10]
Gaps due to
discretization error

FIGURE 18

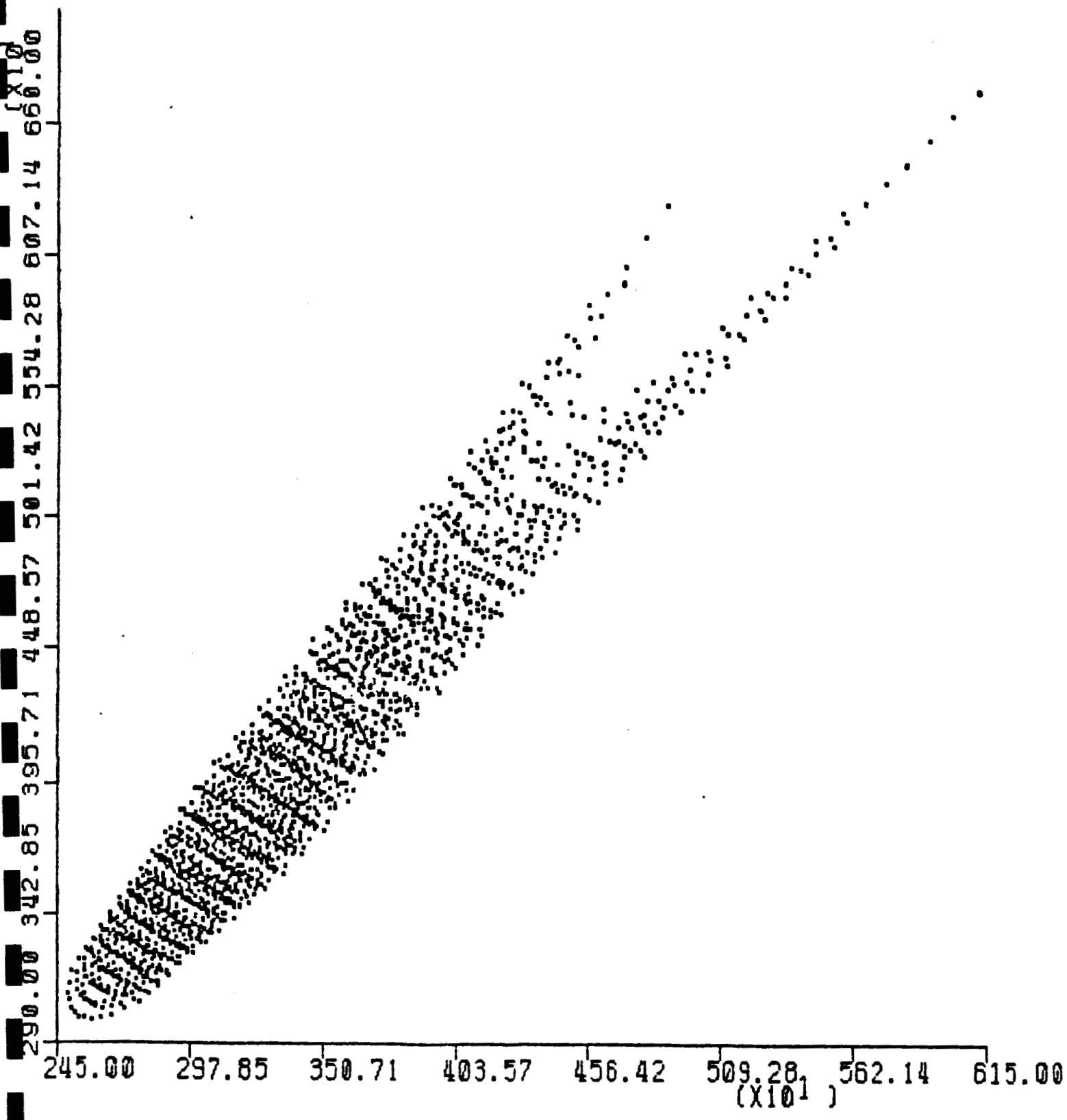
(X10)
660.00
607.14
554.28
501.42
448.57
395.71
342.85
290.00
245.00
297.85
350.71
403.57
456.42
509.28
562.14
615.00
(X10¹)

FIGURE 19

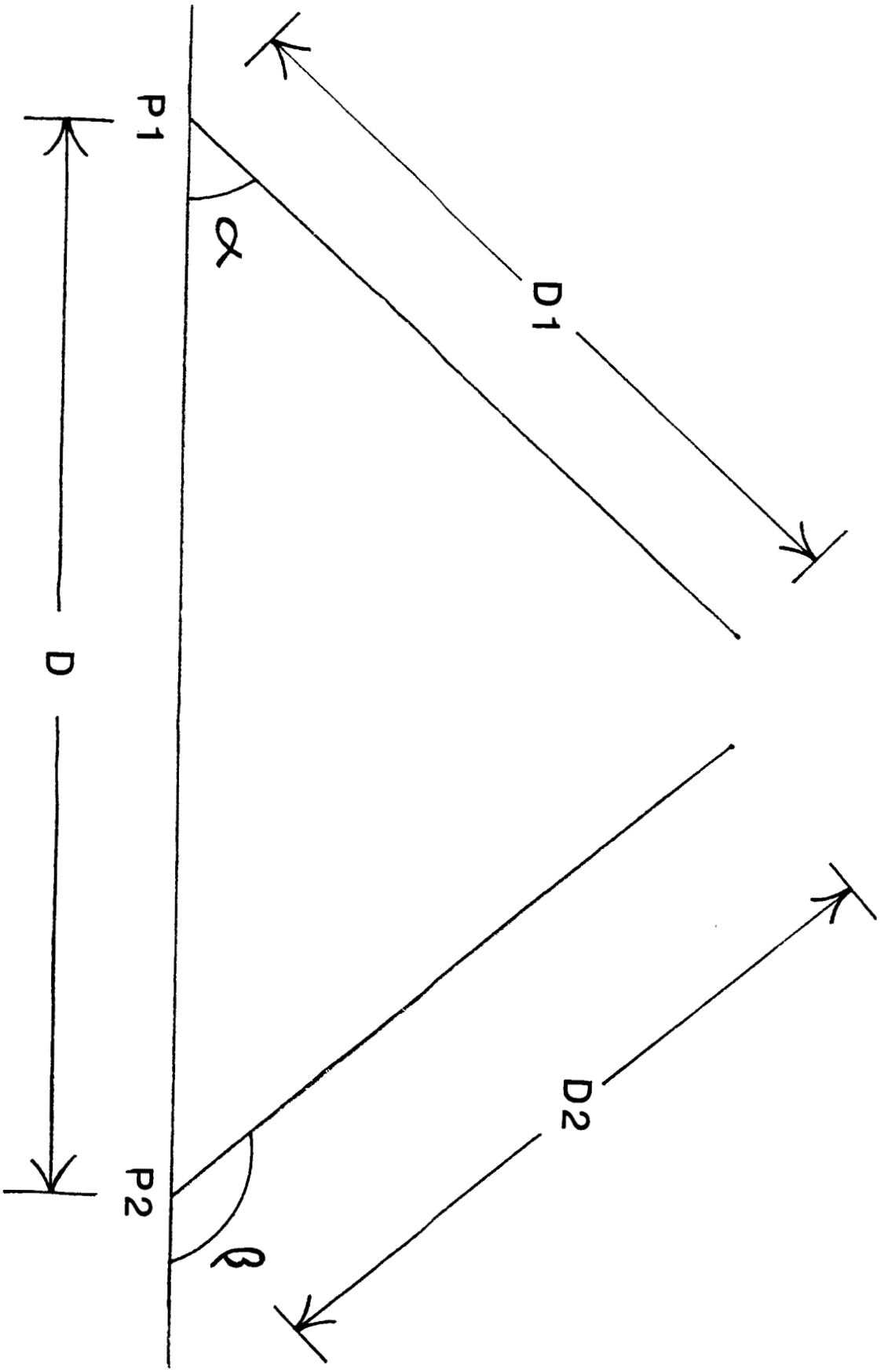

FIGURE 20

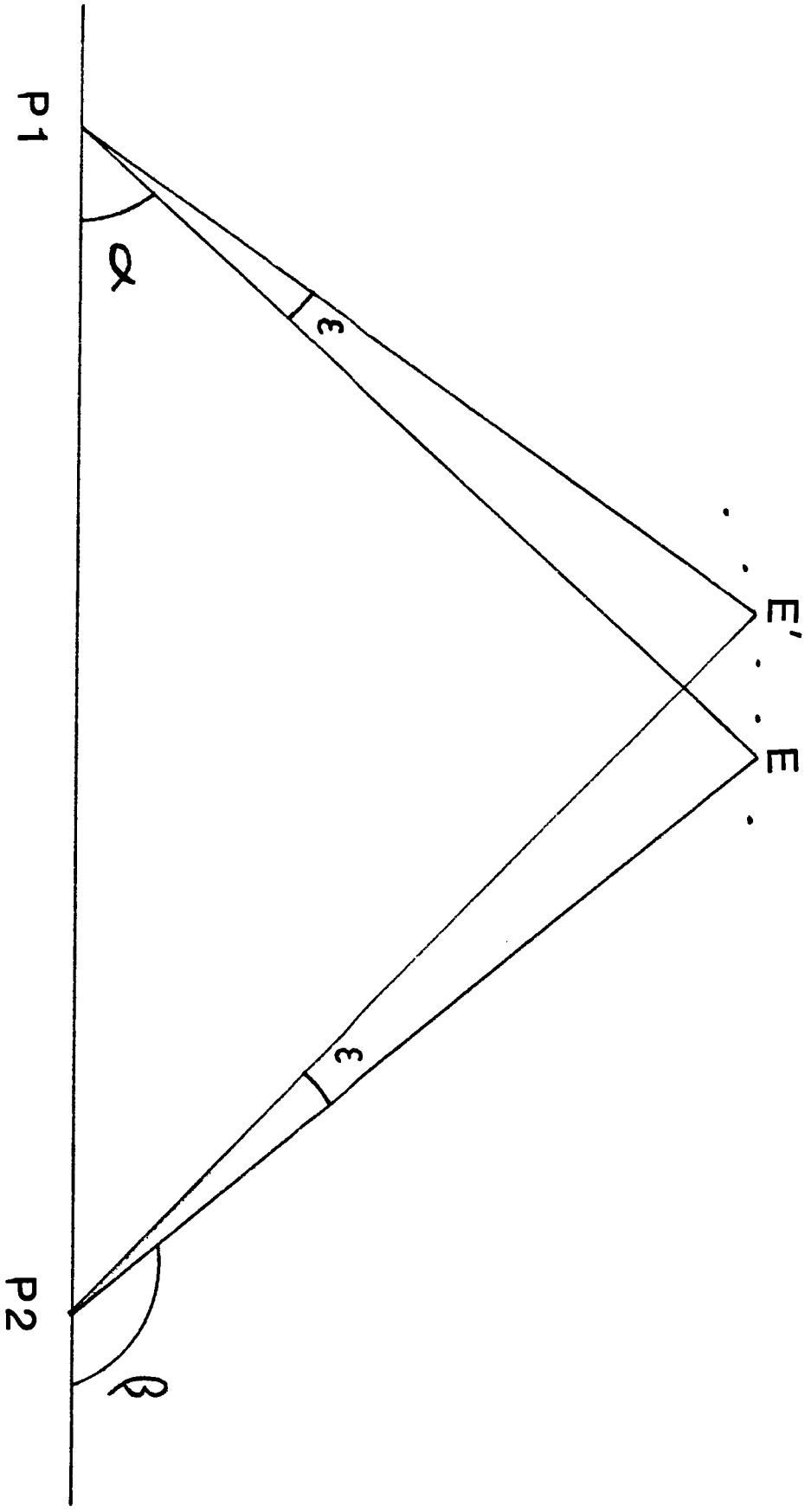

FIGURE 21

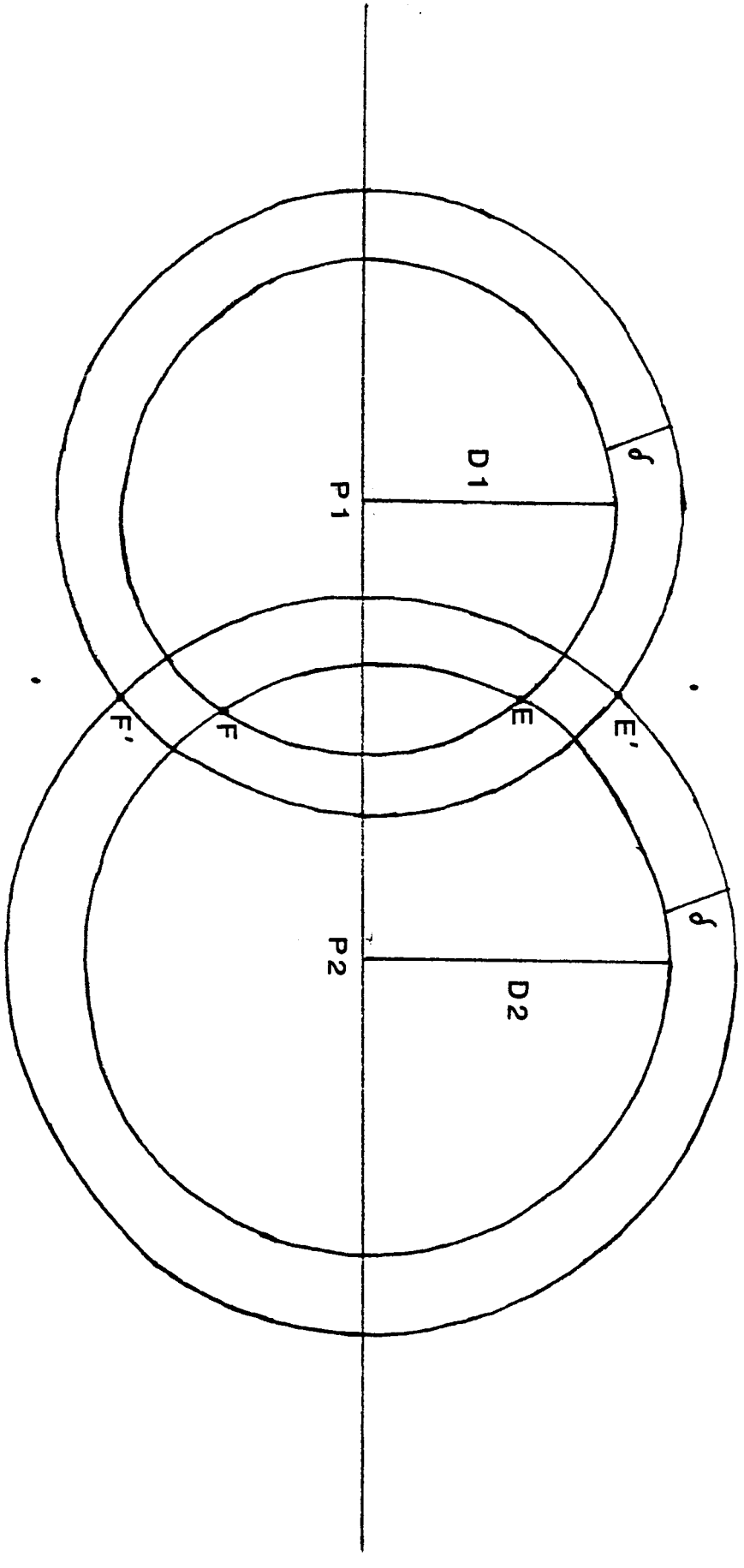

FIGURE 22

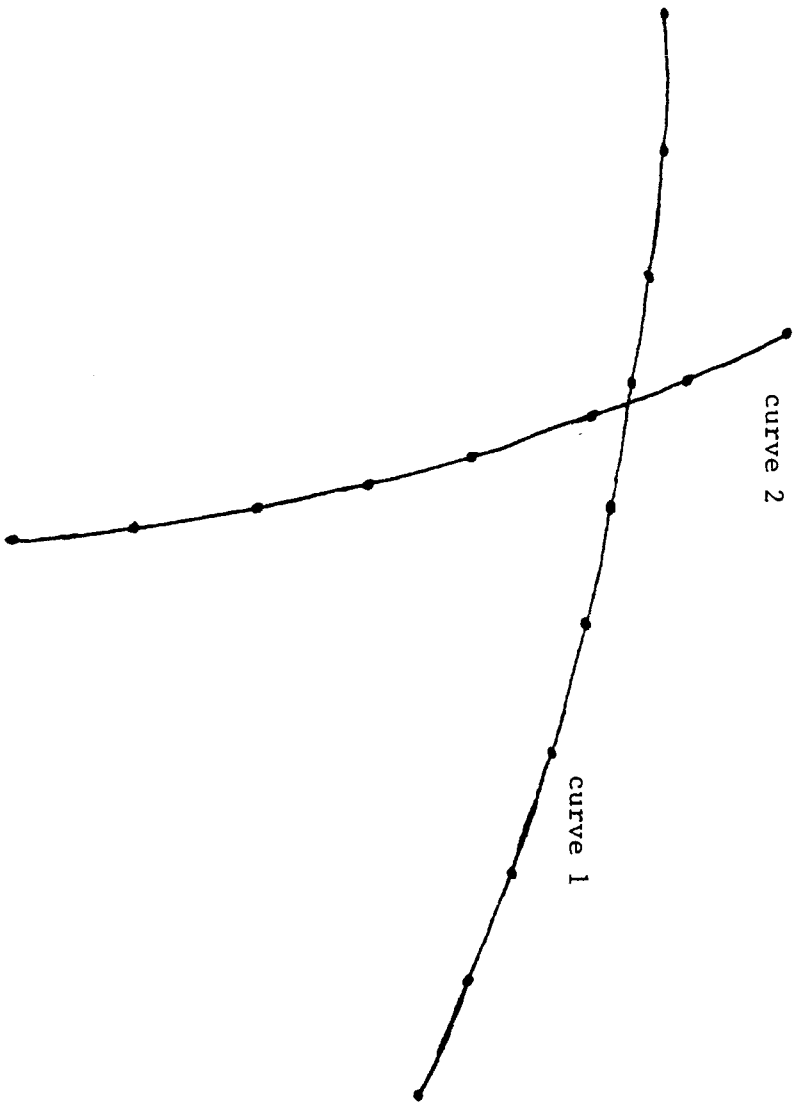

REFERENCES

1. Stansfield, R.G., "Statistical Theory of D.F. Fixing", Journal of the Institution of Electrical Engineering, vol. 94, Part IIIA, March, 1947.

2. Daniells, H.E., "The Theory of Position Finding", The Journal of the Royal Statistical Society, Series B, 13:2, 1951

3. Gething, P.J.D., Radio Direction-Finding, London: Peter Peregrinus Ltd., 1978